

3. Data Acquisition and Correlations (Reporting Category C03)

3.1 Reactor Modeling

Introduction

Modeling of the gasification reactor serves two purposes. On the one hand, the reactor model provides a learning tool by which the reactor performance can be studied and comprehended. On the other hand, the model serves as a predictive tool to provide guidance in the operation of the pilot plant and the design of a commercial unit.

The work described in this section covers four areas: (1) prediction of gasifier fluid bed density; (2) use of bench scale and pilot plant data to improve the reactor model; (3) use of the reactor model to guide PDU operations; and (4) validation of the model using demonstration run data.

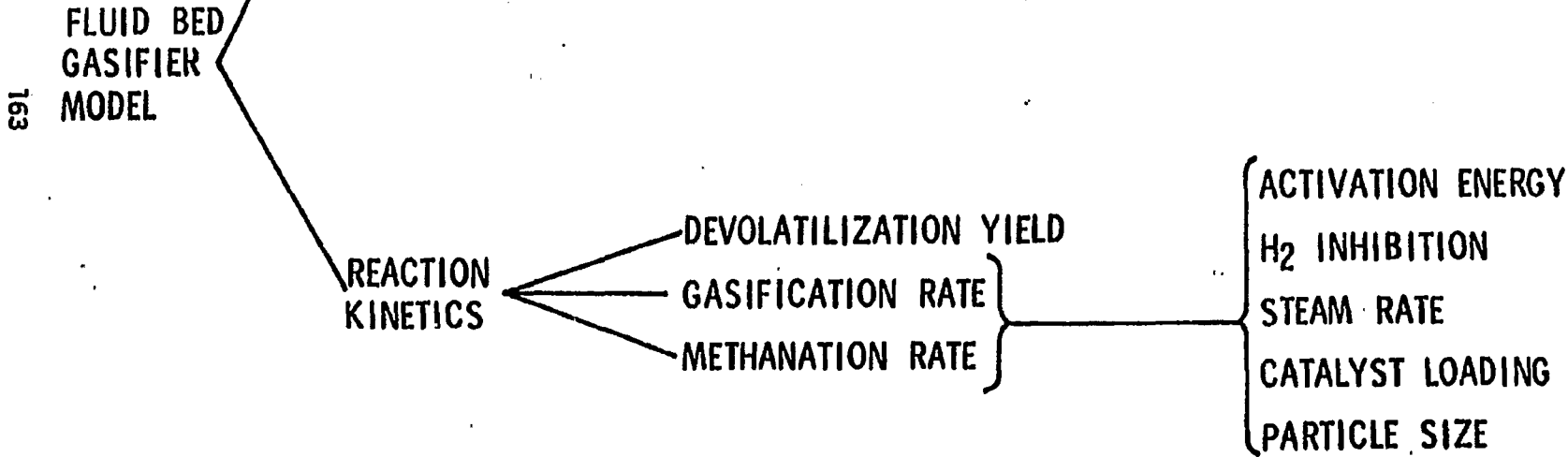
During the predevelopment phase of research on the CCG process (DOE Contract E [49-18]-2369) a preliminary gasifier kinetics and contacting model was developed. This model was used as the starting point during the development phase of research. This article begins with a description of this original, preliminary model.

Original Gasifier Model

The gasification reactor is a fluidized bed of complex hydrodynamics and chemical reactions. Fluidized beds consist of two phases: the emulsion phase (i.e., the dense phase) and the bubble phase. The emulsion phase is a suspension of particles and is the continuous phase. The bubble phase consists of relatively particle-free gas bubbles rising discretely through the emulsion phase. Since the bulk of the gas passes through the bed in the form of bubbles and the gasification and methanation reactions are catalyzed by the potassium loaded char particles, the interchange of gas between the bubble phase and the emulsion phase is an important aspect of fluid bed reactor modeling. Other important aspects in the modeling of the gasification reactor are the intrinsic reaction rates and the coal devolatilization yield. The important elements of the gasification reactor modeling are outlined in Figure 3.1-1.

The model⁽¹⁾ is based on the two-phase theory for fluidized bed reactors. Gas flow at minimum fluidizing velocity percolates through the emulsion phase while the excess gas passes through the bed in the form of bubbles. Small bubbles are formed at the bottom of the bed, and these bubbles coalesce and grow as they rise through the bed until they reach a maximum stable size. For computation, the reactor is segmented into compartments along the axial direction. Within each compartment, each phase is assumed to be well mixed, and mass transfer takes place between the phases in accordance with the correlations proposed by Kunii and Levenspiel.⁽²⁾ For the slugging

FIGURE 3.1-1
ELEMENTS OF CCG GASIFIER MODELING



regime (i.e., bubbles bigger than one-half the reactor diameter) mass transfer is prescribed by Hovmand and Davidson's⁽³⁾ correlations. Figure 3.1-2 shows schematically the organization of the original reactor model. The bases for the major fluidization parameters employed in the model and the kinetic expressions, which have been derived from bench scale fixed bed reactors,⁽⁴⁾ are summarized in Table 3.1-1.

The original reactor model did a reasonable job of predicting performance of the 100 psig Fluid Bed Gasifier (FGB) operated during the predevelopment phase of research. Data from the PDU gasifier and new bench scale data have indicated several areas where improvement could be made. These areas are discussed below.

Bed Density

Bed density measurements made in the PDU reveal that bed expansion is much greater (i.e., bed densities much lower) than can be reasonably predicted from the classical two-phase theory. Figure 3.1-3 illustrates this point. Assuming that the bubble diameters within the PDU range from one-half inch to ten inches, it is seen that most PDU data points fall above the predicted bed expansion based on the two-phase theory.

Though there can be more than one explanation for the observed behavior, one logical explanation found in the literature is that there is a considerable increase in the emulsion phase voidage beyond minimum fluidization. The char particles in the PDU typically have low bulk densities (approximately 30-60 lb/ft³) and contain significant amounts of small particles. By Geldart's classification,⁽⁵⁾ this is a type A particle which is known to give rise to homogenous expansion of the emulsion phase before bubbling begins. It is also known that the emulsion phase expansion will increase with decreasing particle size. This is consistent with the observation in the PDU that bed expansion increases with decreasing particle size as shown in Figure 3.1-4. Figure 3.1-4 also suggests that as particle size increases beyond 250 μm , bed expansion asymptotically approaches that predicted by the two-phase theory.

The two-phase theory used in the present model is found to significantly overpredict the bed density when the particle sizes are small. For an average particle size of 250 μm or greater, the two-phase theory appears to provide a reasonable approximation. For particles smaller than 250 μm the following modifications in the calculating bed densities can be made.

From mass balance:

$$\rho_{\text{bed}} = \left[\frac{U_b}{(U - U_e) + U_{b,\infty}} \right] (1 - \epsilon_e) \rho_f \quad (3.1-1)$$

where: $\rho_{\text{bed}}, \rho_p$ = fluid bed and particle densities, respectively.
 $U_b, U_{b,\infty}$ = isolated bubble rise velocity
 U, U_e = total and emulsion phase superficial velocities respectively
 ϵ_e = emulsion phase voidage

FIGURE 3.1-2

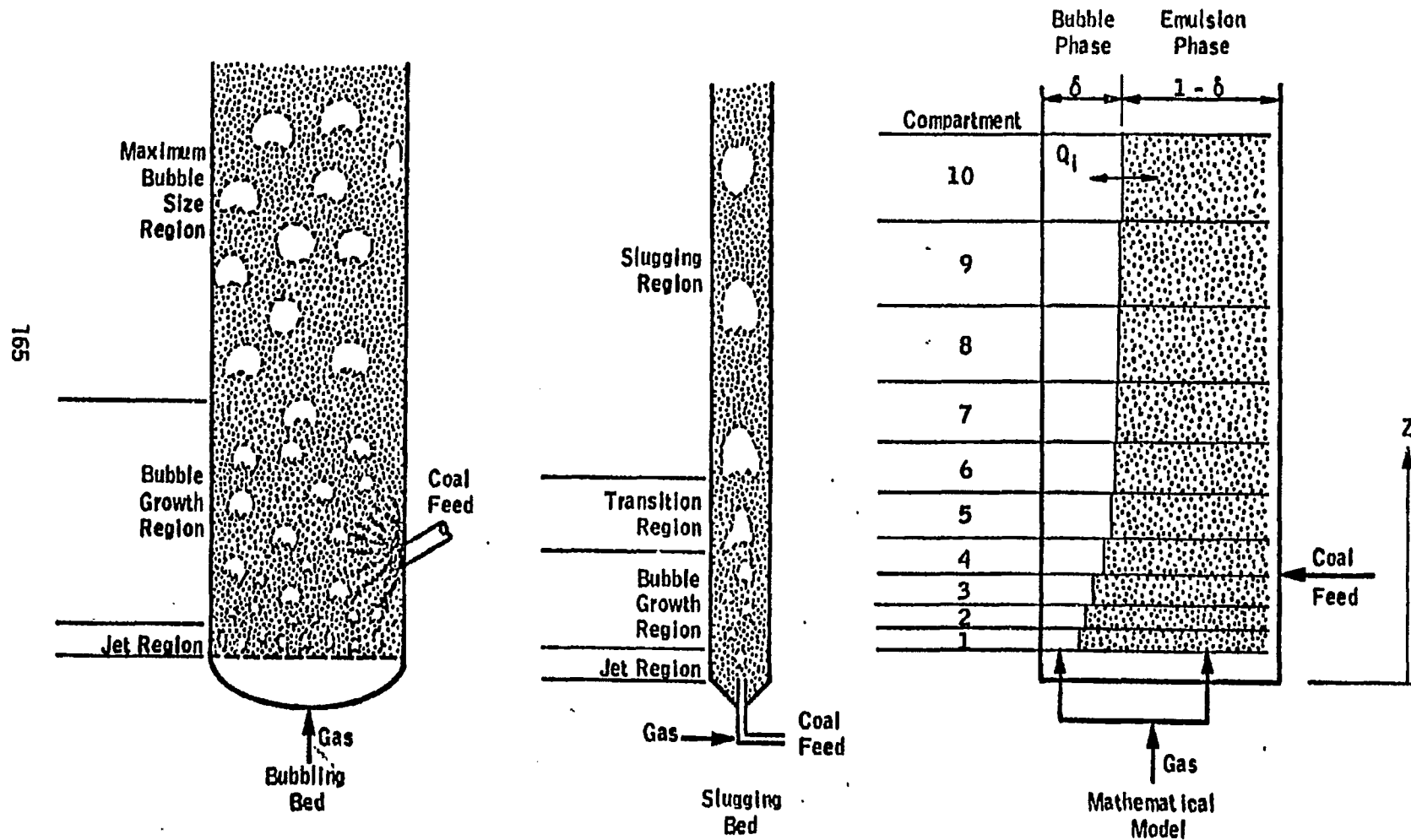
CONCEPTUAL REPRESENTATION OF FLUID BED REACTOR MODEL

Table 3.1-1
FLUIDIZATION PARAMETERS AND KINETIC EXPRESSIONS
USED IN THE PRESENT MODEL

<u>Parameter</u>	<u>Source or Expression</u>
Minimum Fluidizing Velocity (U_{mf})	Ergun equation
Jet height above distributor	Mori and Wen correlation
Bubble growth	Geldart's correlation
Maximum stable bubble size	Modified Davidson-Harrison correlation
Interphase Mass Transfer for Bubbles	Kunii and Levenspiel's correlation
Slugging bed mass transfer	Hovmand and Davidson's correlation
Gasification Rate	$r_G = \frac{6.8 \times 10^7 \exp(-15,100^\circ\text{K}/T) f_g C_k [P_{H_2O} - \frac{P_{CO} P_{H_2}}{K_G}]}{P_{H_2} + 0.21 P_{CO} P_{H_2} + 0.0595 P_{H_2O}}$
Methanation rate	$r_M = \frac{1.99 \times 10^6 \exp(-14,190^\circ\text{K}/T) f_M C_k [P_{H_2} P_{CO} - P_{CH_4} P_{H_2O} / K_M]}{1 + 7.95 P_{H_2}}$
Devolatilization yield	Gibson-Euler correlation for uncatalyzed coal

FIGURE 3.1-3

PDU BED EXPANSION EXCEEDS THAT PREDICTED
BY THE CLASSICAL TWO-PHASE THEORY

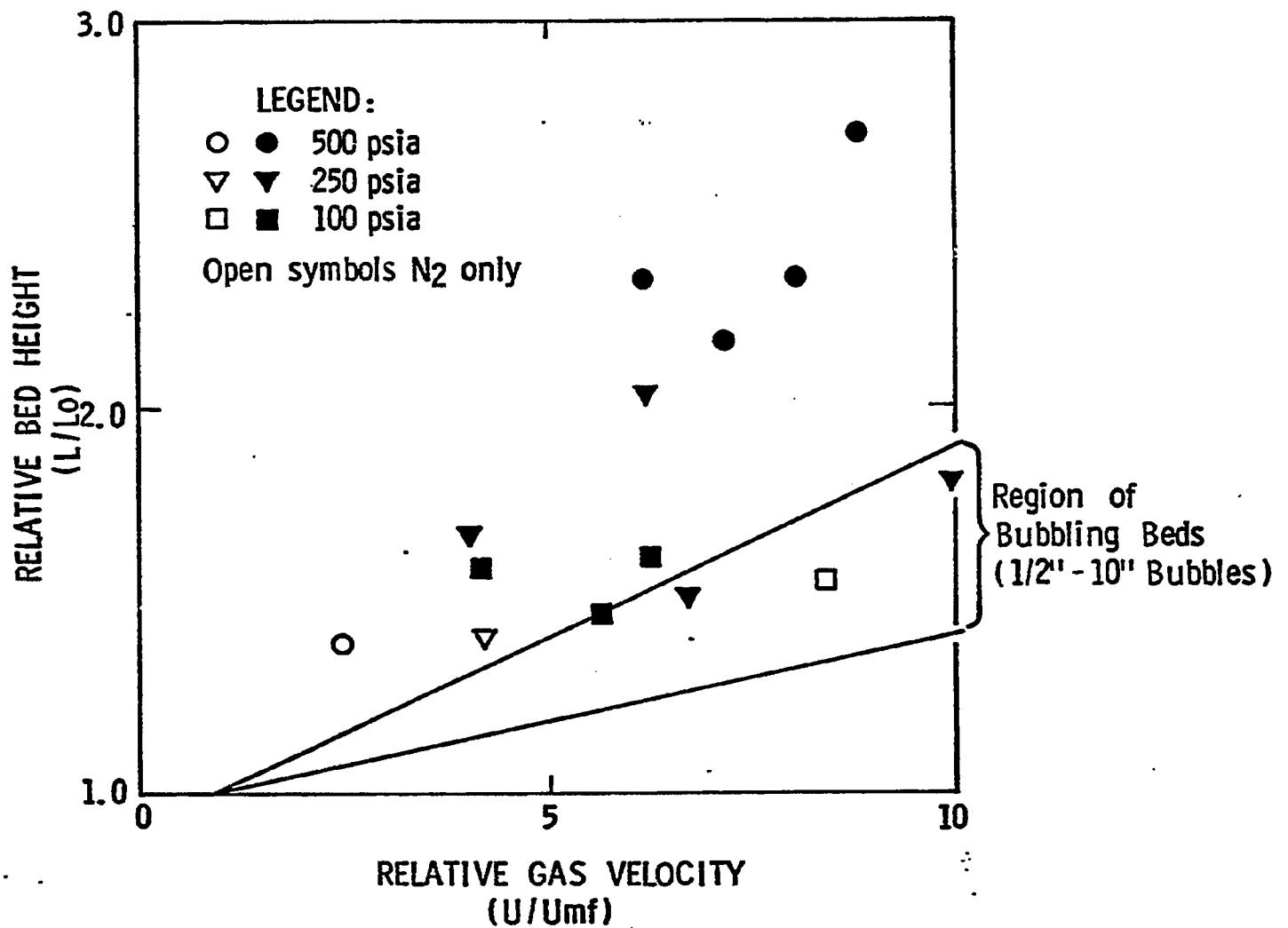
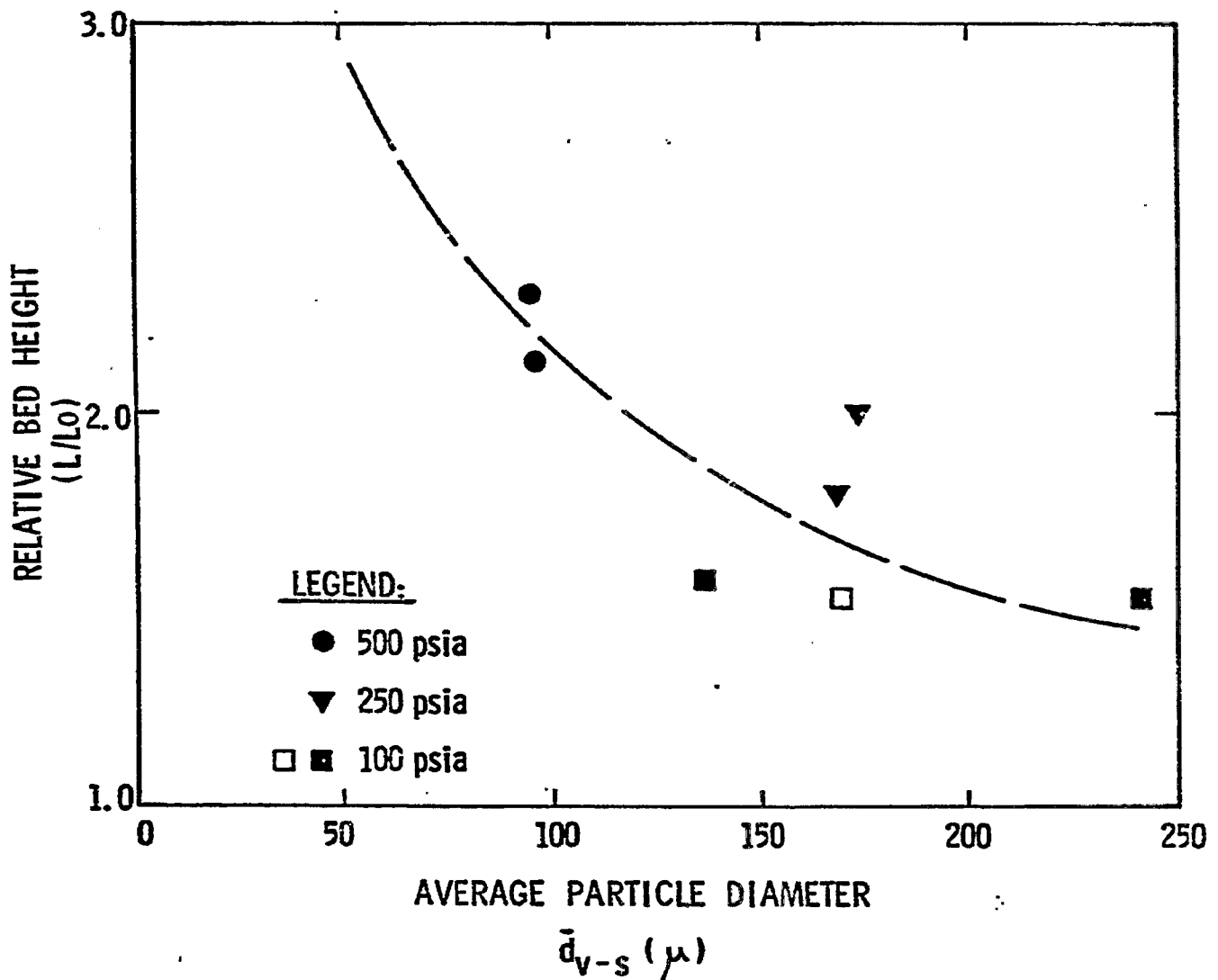


FIGURE 3.1-4

BED EXPANSION STRONGLY DEPENDENT ON PARTICLE SIZE

5360-002GFbw

The bubble rise velocity is related to the estimate of bubble size which is discussed later in this section of the report. The unknown quantities ϵ_e and U_e can be estimated from the following correlations:

From Geldart and Abrahamson (6)

$$\frac{U_{mb}}{U_{mf}} = \frac{4.1 \times 10^4 \mu^{0.9} \rho^{0.1}}{(\rho_p - \rho) g \bar{d}_p} \quad (3.1-2)$$

Assuming the emulsion gas velocity, U_e , and the minimum bubbling velocity, U_{mb} , are approximately equal then:

$$U_e \approx U_{mb} \quad (3.1-3)$$

and applying the Richardson-Zaki correlation (7) for voidage:

$$\frac{U_e}{U_t} = \epsilon^{4.7} \quad (3.1-4)$$

The following relationship can be derived:

$$\frac{U_e}{U_{mf}} = \left(\frac{\epsilon_e}{\epsilon_{mf}} \right)^{4.7} \quad (3.1-5)$$

Combining equations (3.1-5) and (3.1-2) to give:

$$\frac{\epsilon_e}{\epsilon_{mf}} = \frac{4.1 \times 10^4 \mu^{0.9} \rho^{0.1}}{(\rho_p - \rho) g \bar{d}_p} \quad (3.1-6)$$

Equations 3.1-6 and 3.1-5 can be used to estimate ϵ_e and U_e respectively, and bed density can be estimated by Equation 3.1-1. This will result in better estimation of bed density since it allows for the increase in the emulsion phase voidage. In so doing, it also allows for a greater amount of gas flowing through the emulsion phase (i.e., $U_e > U_{mf}$) and this marks another departure from the present model.

Bubble Size

The importance of bubble size and mass transfer between the bubble and the emulsion phases is illustrated in Figure 3.1-5. Figure 3.1-5 shows the calculated relative reactor volume as a function of bubble size using the original model. Conversely, for a given reactor size, increasing bubble size will result in lower carbon conversion, as shown in Figure 3.1-6. Bubbles undergo coalescence as they rise in the bed, resulting in bigger bubbles. In principle, bubbles can keep coalescing and growing until limited by vessel size or the total amount of gas fed into the system. For fine particles, however, an equilibrium size is often reached, beyond which, the incidence of bubble splitting limits the bubble growth.

Figure 3.1-5

COMMERCIAL GASIFIER VOLUME INCREASES WITH BUBBLE SIZE

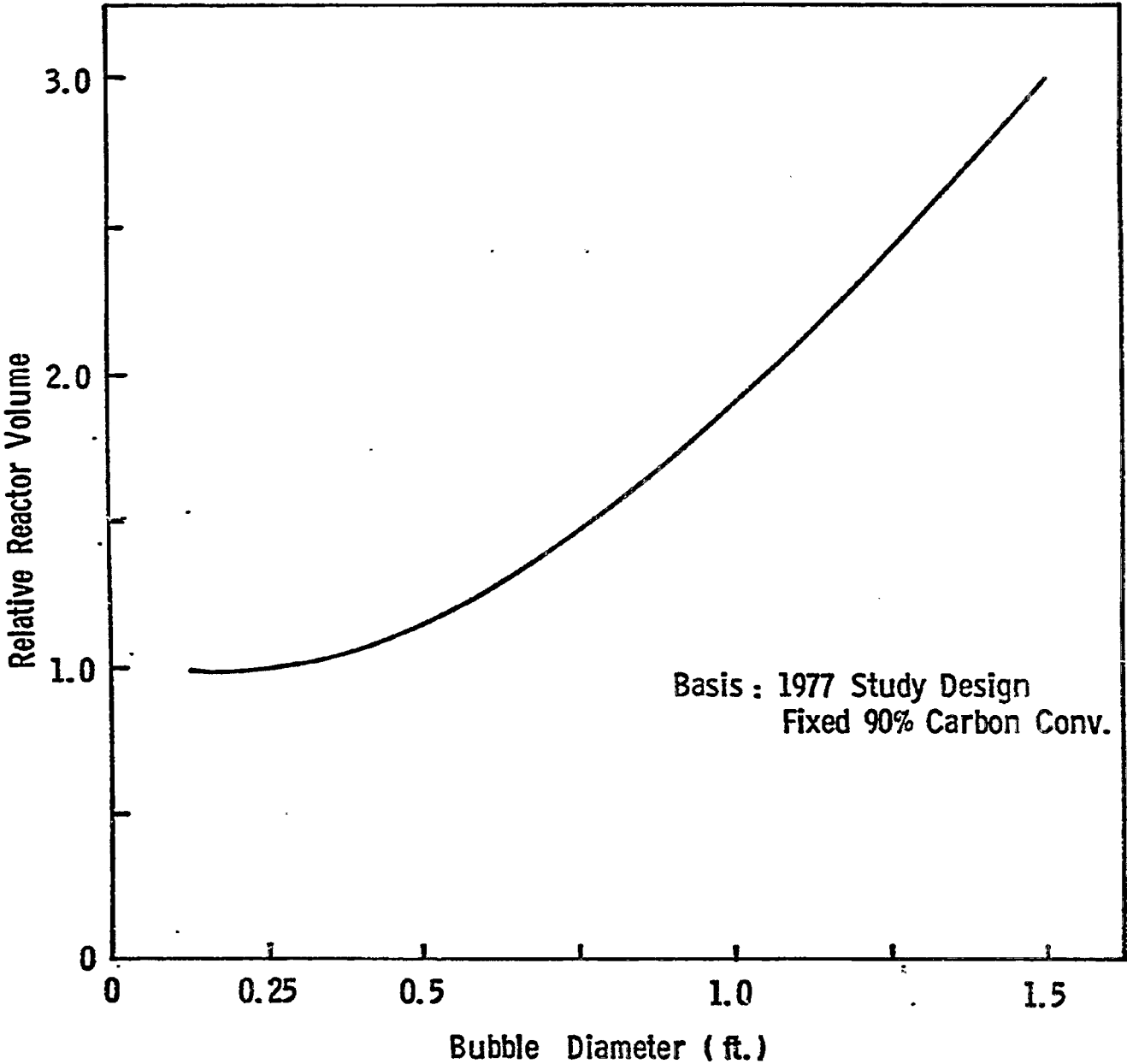
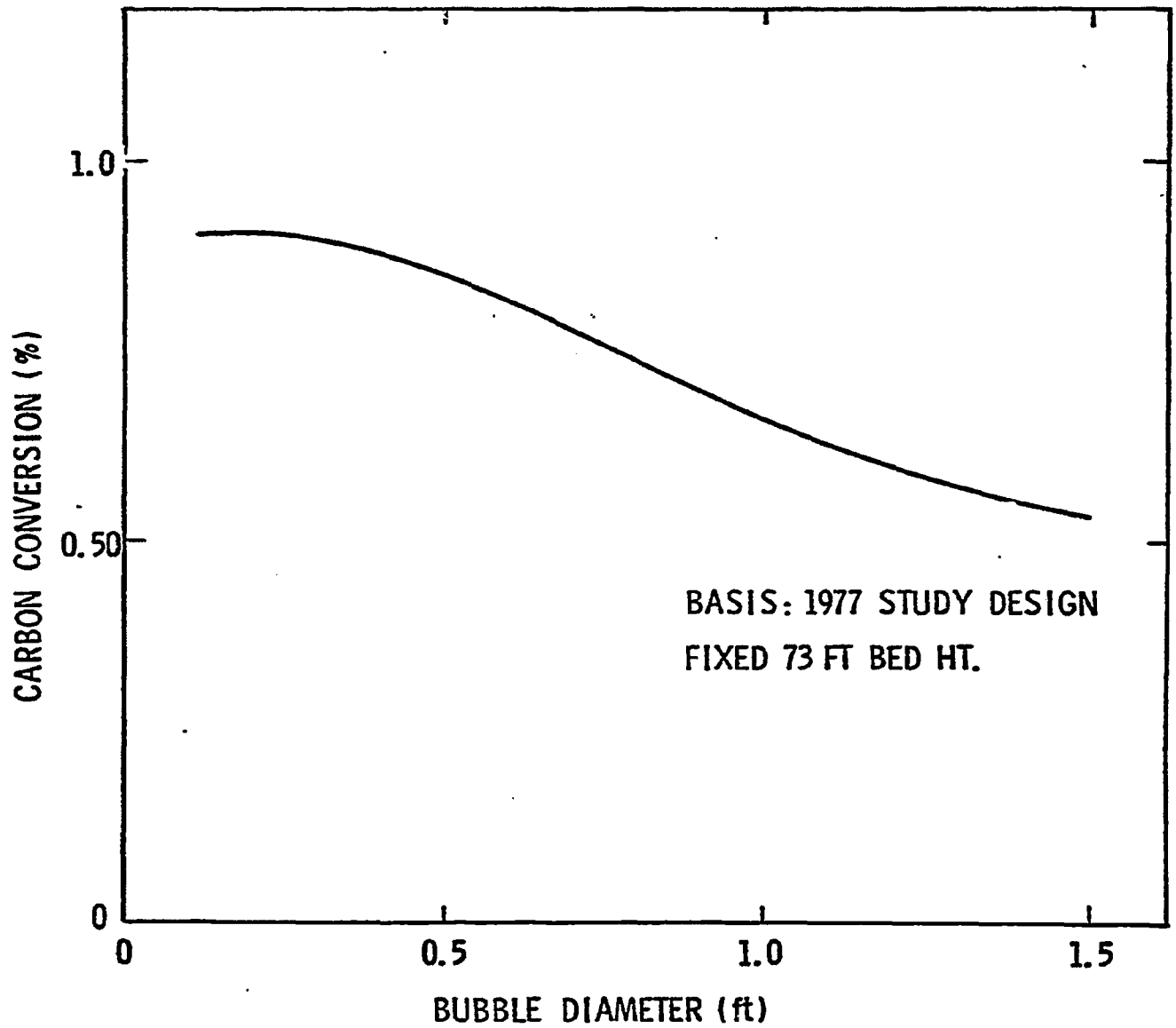


FIGURE 3.1-6
EFFECT OF BUBBLE SIZE ON FEED CARBON CONVERSION



The original model used Geldart's(8) correlation for bubble growth as a function of bed height. Advances in recent years indicate that the more conservative growth rates proposed by Rowe(9) and Darton, et al(10) may be more realistic. Figure 3.1-7 shows the comparison of the three correlations of bubble size. The close agreement between Rowe's X-ray based correlation and that of Darton, et al., which is theoretically derived, lends support to their correlations.

The equilibrium bubble size, or the maximum bubble size, is difficult to estimate. The Harrison-Davidson-DeKock maximum stable bubble hypothesis(11) postulates that when the gas velocity inside a bubble exceeds the terminal velocity of the particle, the bubble will be destroyed by particles carried into the void by gas. By analogy to gas bubbles in a liquid medium, they assumed that the gas velocity within a bubble in a fluidized bed is approximately equal to the rising velocity of the bubble. Thus, the bubble will be obliterated if:

$$U_b = U_t$$

Since: $U_b = 0.71 \sqrt{gd_b}$

then: $(d_b)_{\max} = \left(\frac{U_t}{0.71} \right)^2 \frac{1}{g}$

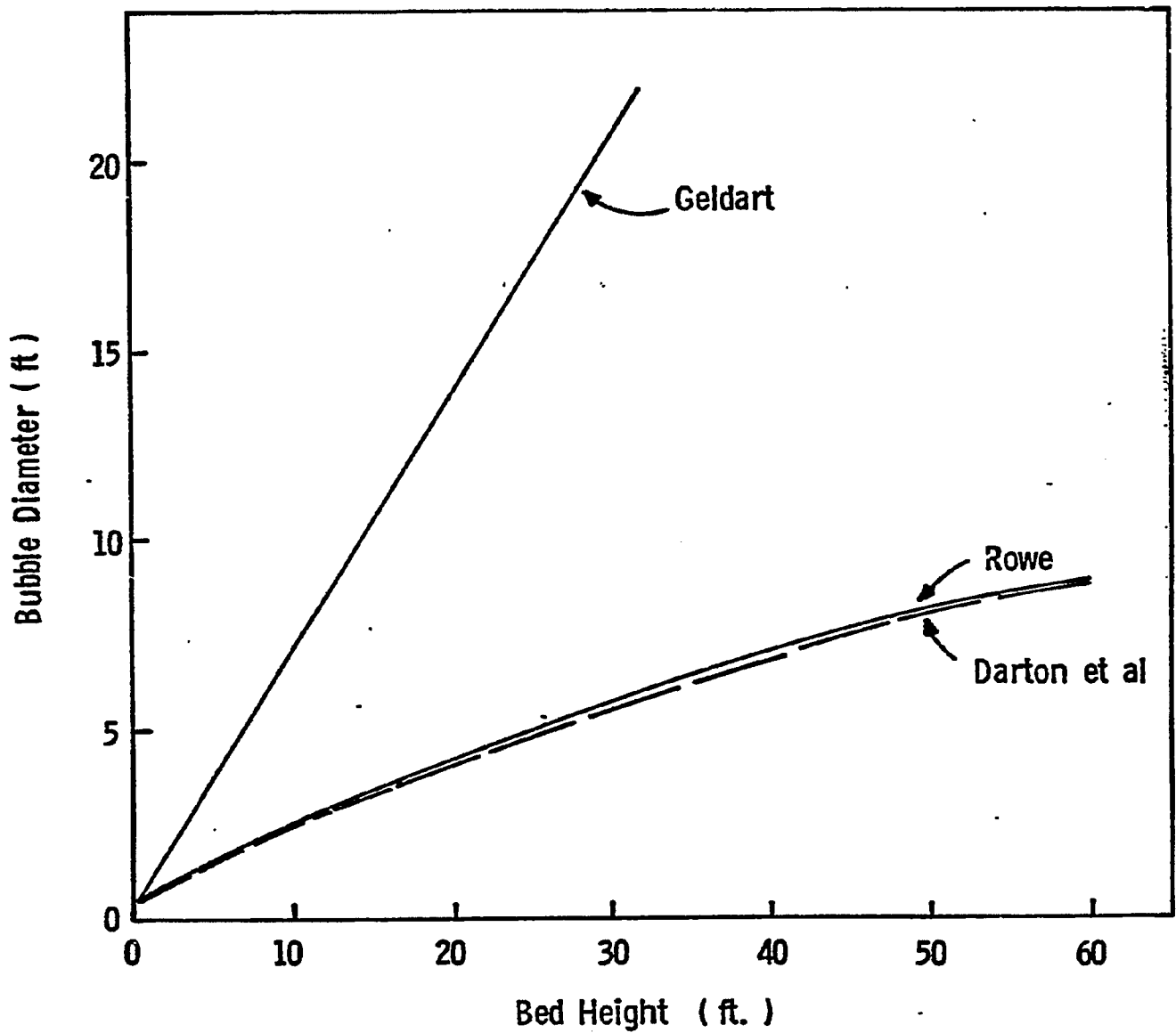
An alternative approach to the question of bubble stability is to examine the Taylor instability of the bubble roof as done by Clift, et al(12). Their analyses indicate that bubble instability is primarily a function of the effective kinematic viscosity of the emulsion phase. Unfortunately, there is at present no universally accepted way of estimating the maximum bubble size. Bubble size determination is an area where further experimental data are needed.

Reaction Kinetics from Bench Scale Data

The kinetics of the steam-carbon reaction were studied extensively in bench scale reactors to elucidate a number of issues. The experimental set-up and other details are given in Section 4.1 of this report.

BUBBLE GROWTH WITH BED HEIGHT : COMPARISON OF CORRELATIONS

(Based on Commercial Gasifier Conditions)



It was found that an activation energy of 50 kcal/g mole $^{\circ}$ K gives a much better fit to the mini-gasifier data than the 30 kcal/g mole $^{\circ}$ K number used in the original model. This is shown in Figure 3.1-8. Another improvement can be made in the area of catalyst loading. The gasification rate increases linearly with the water soluble K to C atom ratio up to about 0.2 and remains constant with further increase in K/C ratio. The coefficient f_G in the gasification rate expression can be modified to reflect this behavior. This is shown in Figure 3.1-9. An additional area of modification lies in the inhibition terms. Regression of fixed bed data at various pressures indicated that the data could be estimated by the following gasification rate expression:

$$r_G = \frac{k_G \exp(-50,000/RT) f_G C_K [P_{H_2O} - P_{H_2} P_{CO}/K_G - a]}{(P_{H_2} + 0.18 P_{H_2O})}$$

All the modifications described above were combined into the new CCG model version. Table 3.1-2 compares the experimentally measured gasification rates with those calculated by both the original and the modified models. With the exception of one group of data, the comparison shows that the modified model provides a better fit to the experimental rates. Attempts were then made to further refine the model and demonstrate its applicability to the FBG and PDU data.

Incorporation of Pilot Plant Data

The methanation rate expression used in the original model had the following form:

$$r_M = \frac{2 \times 10^6 \exp(-28,200/RT) C_K [P_{H_2}^3 P_{CO} P_{CH_4} P_{H_2O}/K_M]}{(1 + 8 P_{H_2})}$$

While this expression appeared to fit the FBG data, it consistently over-predicts methane production for the PDU runs at 265 psia and 500 psia pressure levels. This over-prediction is attributed to the fact that in this expression, the rate of methane formation is overly dependent on the total pressure of the system.

Expressions with a lesser dependence on total pressure were therefore sought. The following methanation expression was found to give good fit to all these pressure levels (i.e., 100, 265, 500 psi):

FIGURE 3.1-8

MINI-GASIFIER DATA CAN BEST BE APPROXIMATED BY AN
ACTIVATION ENERGY OF 50 KCAL/G MOLE

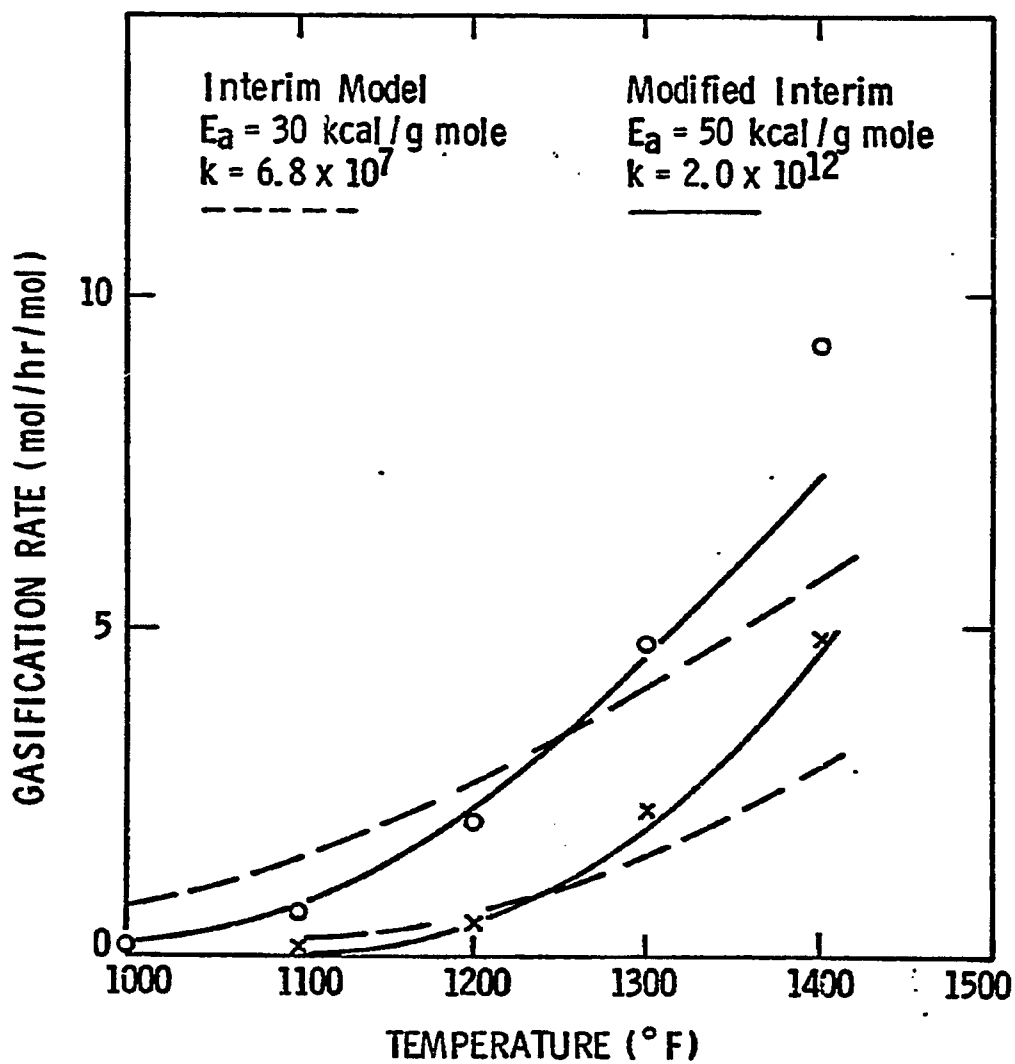


FIGURE 3.1-9
COMPARISON OF THE f_G TERMS IN THE
GASIFICATION RATE EXPRESSION

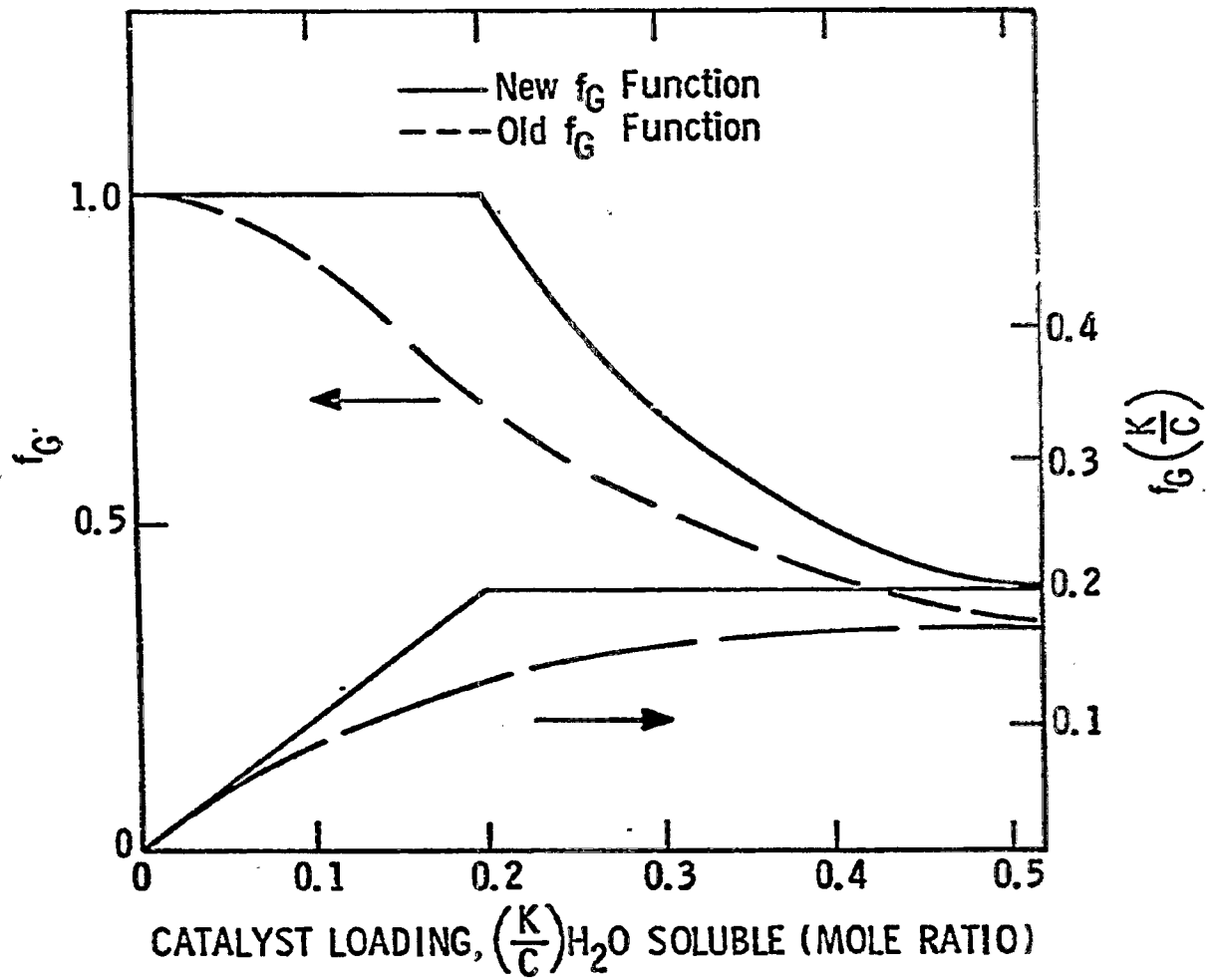


Table 3-1-2

SIMULATION OF MINI-BED RUNS

Series**	Run No.	Exp'l Rate (hr-1)	Original Model	Modification* Model
A	1	5.3	4.1	5.0
	2	4.2	2.7	3.4
	3	3.6	2.2	2.9
	4	3.3	1.5	2.0
	5	2.4	1.0	1.4
	6	1.7	0.9	1.2
B	1	5.1	4.2	5.0
	2	3.9	3.1	3.9
	3	2.9	2.2	2.9
	4	2.2	1.5	2.0
	5	2.0	1.0	1.3
	6	1.8	0.7	0.9
C	1	1.6	1.3	1.3
	2	2.6	2.0	2.3
	3	3.1	2.7	3.2
	4	3.6	3.2	3.7
	5	4.6	4.2	5.0
	6	6.7	6.1	7.6
D	1	0.13	0.71	0.44
	2	0.56	1.50	1.17
	3	2.04	2.64	2.60
	4	4.74	4.1	4.90
	5	9.3	5.7	7.5
E	1	0.08	0.23	0.09
	2	0.49	0.62	0.50
	3	2.22	1.50	2.0
	4	4.80	2.80	4.86
F	1	3.3	3.5	4.0
	2	2.4	2.8	3.1
	3	3.0	3.0	3.4
	4	5.1	4.1	4.9
	5	5.1	5.8	6.6
	6	6.1	8.2	9.1
	7	5.2	5.2	6.2
	8	4.9	4.1	5.0
	9	5.7	5.4	6.2
	10	6.2	6.5	7.7
G	1	1.4	1.2	1.4
	2	0.6	0.9	1.0
	3	1.2	1.1	1.2
	4	2.2	1.5	2.0
	5	2.7	2.1	2.5
	6	2.7	2.5	2.7
	7	2.1	1.8	2.4
	8	2.4	1.6	2.2
	9	2.5	2.0	2.4
	10	2.1	2.0	2.6

*Modification of original Model as follows:

$$(i) f_G = 1.0 \text{ for } K/C \leq 0.2$$

$$f_G = 0.2 / \frac{K}{C} \text{ for } K/C > 0.2$$

$$(ii) E_a = 50 \text{ k cal/g mole}$$

$$k = 2 \times 10^{12}$$

**Series A and B - Variations of H₂O/H₂ ratio

Series C - Variations of H₂O/C ratio

Series D and E - Temperature variation, H₂O only and H₂O/H₂ mixture

Series F and G - Variations of K/C ratio with H₂O only and H₂O mixture.

$$r_M = \frac{3.5 \times 10^6 \exp(-28,200/RT) C_K [P_{H_2}^3 P_{CO} - P_{CH_4} P_{H_2O}/K_M]}{(1 + 10 P_{H_2}^2)}$$

This new rate expression was used along with the modified gasification expression to simulate selected yield periods from the FBG and PDU data set. Only data points representing 80% or higher carbon conversion and 10 lb/ft³ or higher bed density were compared with the model predictions. Figure 3.1-10 shows the comparison of calculated and experimental carbon and steam conversions over this set of data. Figure 3.1-11 shows the comparison of methane yield for the same set of data. The agreement appears to be satisfactory.

Table 3.1-3 summarizes the major changes made to the CCG Gasifier Reactor Model during the period of research covered by this report.

Pilot Plant Guidance

A systematic set of computer simulations were completed to predict the performance of the PDU gasifier at 500 psia. The gasifier temperature profile assumed was similar to that measured in PDU Yield Period Number 8 (with an average temperature of 1275°F). In all runs, it was assumed that Illinois No. 6 coal impregnated with 12.5% KOH will be used as the feed solid. Carbon conversion was 90% and syngas was balanced (i.e., the amount of H₂ and CO going into and coming out of the gasifier were equal). Bed density was assumed to be approximately 15 lb/ft³. Three levels of solids feed rates were used: 80, 100, and 120 lbs (coal and catalyst) per hour. For each solids feed rate, three levels of steam feed rate were used, corresponding to H₂O/C molar feed ratios of 1.25, 1.50, and 1.80. Thus, a total of nine cases were studied.

Three key variables were monitored as the output of the computation. These were: steam conversion, % CH₄ in dry product gas, and the required bed height. Figure 3.1-12 shows that steam conversion is a function of the H₂O/C molar ratio in the feed and it decreases steadily with increasing H₂O/C ratio. Figure 3.1-13 shows that % CH₄ in the dry product gas decreases linearly with increasing H₂O/C ratio. Since it is desirable to have high CH₄ formation rate as well as high steam conversion, results in Figures 3.1-12 and 3.1-13 point to the direction of reducing the H₂O/C ratio in the PDU feed to accomplish these objectives. Figure 3.1-14, however, points out the penalty in moving in this direction. Figure 3.1-14 indicates that for any given solids feed rate, the required bed height to accomplish 90% carbon conversion increases with decreasing ratio of (H₂O/C). Furthermore, the shape of the curves indicate that as H₂O/C ratio is decreased below 1.5, gasifier size is increased dramatically.

FIGURE 3.1-10

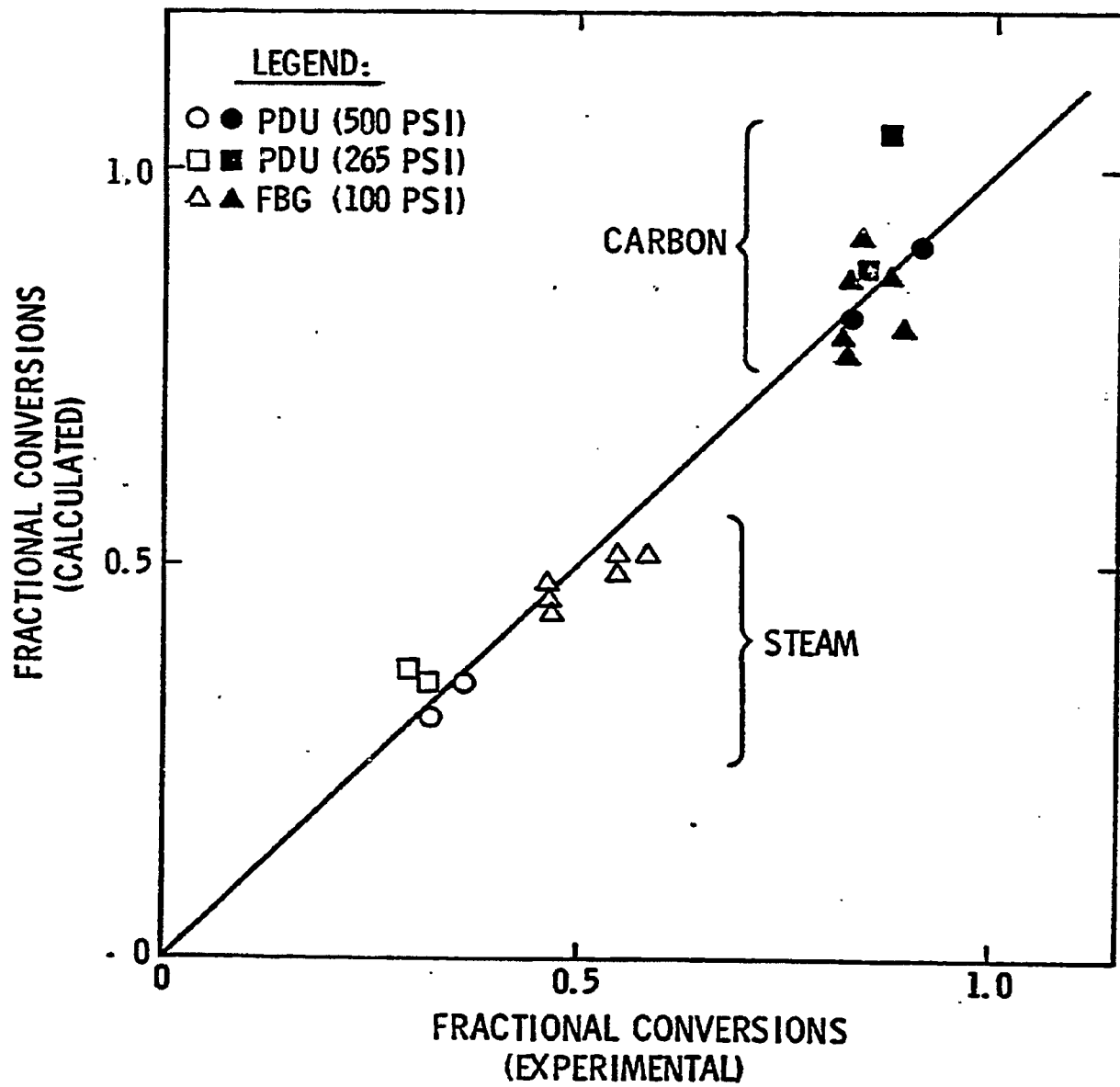
MODEL SIMULATION OF PDU/FBG RUNS:
STEAM AND CARBON CONVERSIONS

FIGURE 3.1-11
MODEL SIMULATION OF PDU/FBG RUNS:
PERCENT CH₄ IN DRY PRODUCT GAS

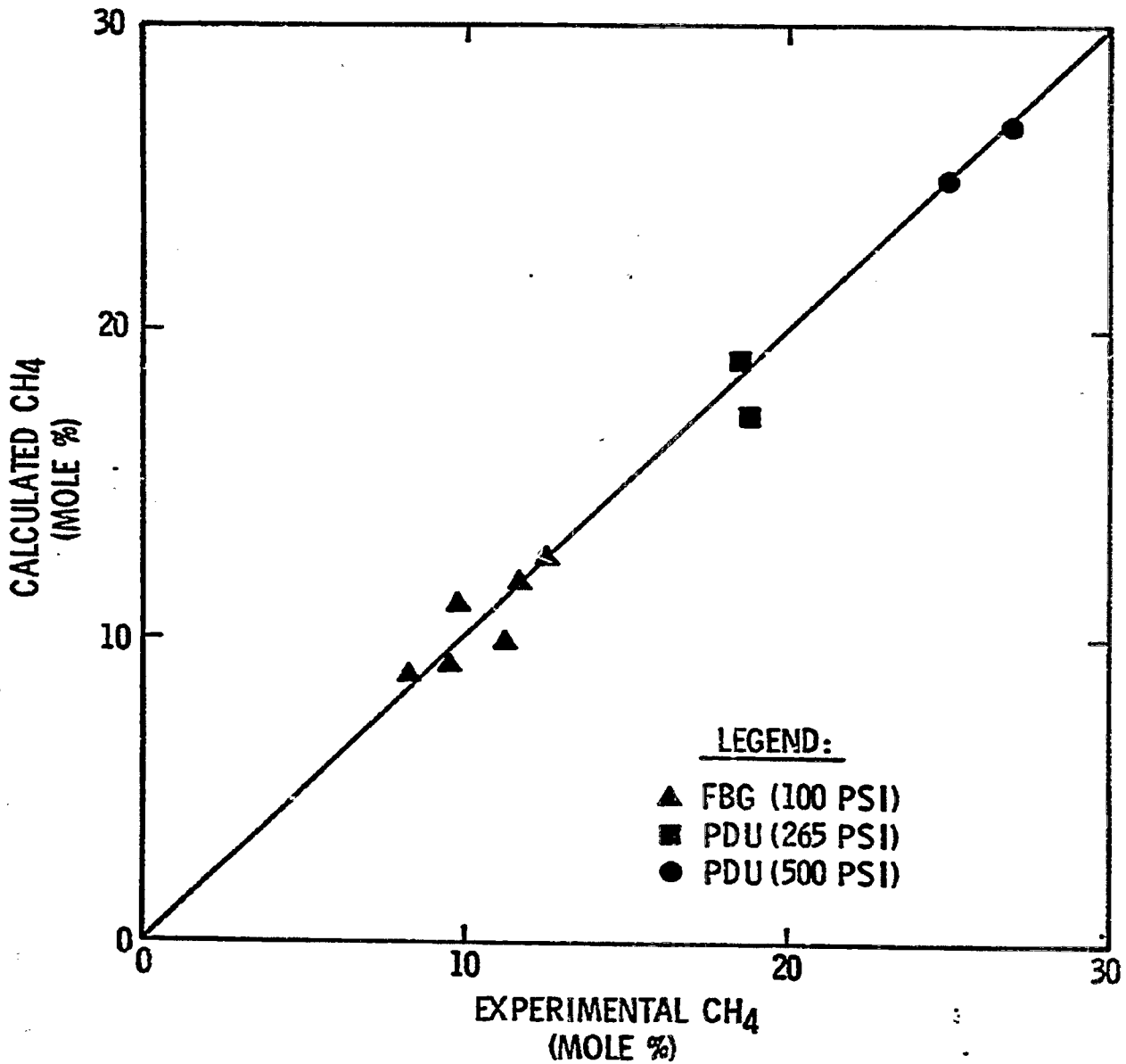


Table 3.1-3

SUMMARY OF MODIFICATIONS MADE TO THE GASIFIER MODEL

Area of Modification	Original Model	Modified Model
Jet penetration distance	Mori-Wen correlation	Bubble formation at Grid plate assumed
Bubble Growth with Bed Height	Geidart's correlation	Rowe's correlation
Maximum Bubble Size	Harrison-Davidson type correlation	Harrison-Davidson type correlation
Fluid Bed Density	Classical two-phase theory	Emulsion phase voidage allowed to increase
Activation energy for Gasification reaction	30 kcal/g mole	50 kcal/g mole
Gasification Kinetic constant	6.8×10^7	2.0×10^{12}
Gasification Inhibition term	$P_{H_2} + 0.21 P_{CO}P_{H_2} + 0.0595 P_{H_2O}$	$P_{H_2} + 0.18 P_{H_2O}$
K/C effect on Gasification Rate	$f_G = 1 - \exp \frac{-0.22}{\frac{K}{C}}$	$f_G = 1.0$ for $\frac{K}{C} \leq 0.2 = \frac{0.2}{\frac{K}{C}}$ for > 0.2
Methanation Inhibition Term	$1 + 8 P_{H_2}$	$1 + 10 P_{H_2}^2$
Methanation rate constant	2×10^6	3.5×10^6
K/C effect on methanation rate	$f_m = 1.0$	$f_m = f_G$

FIGURE 3.1-12
STEAM CONVERSION DEPENDS ON FEED RATIO
MODEL SIMULATION OF PDU

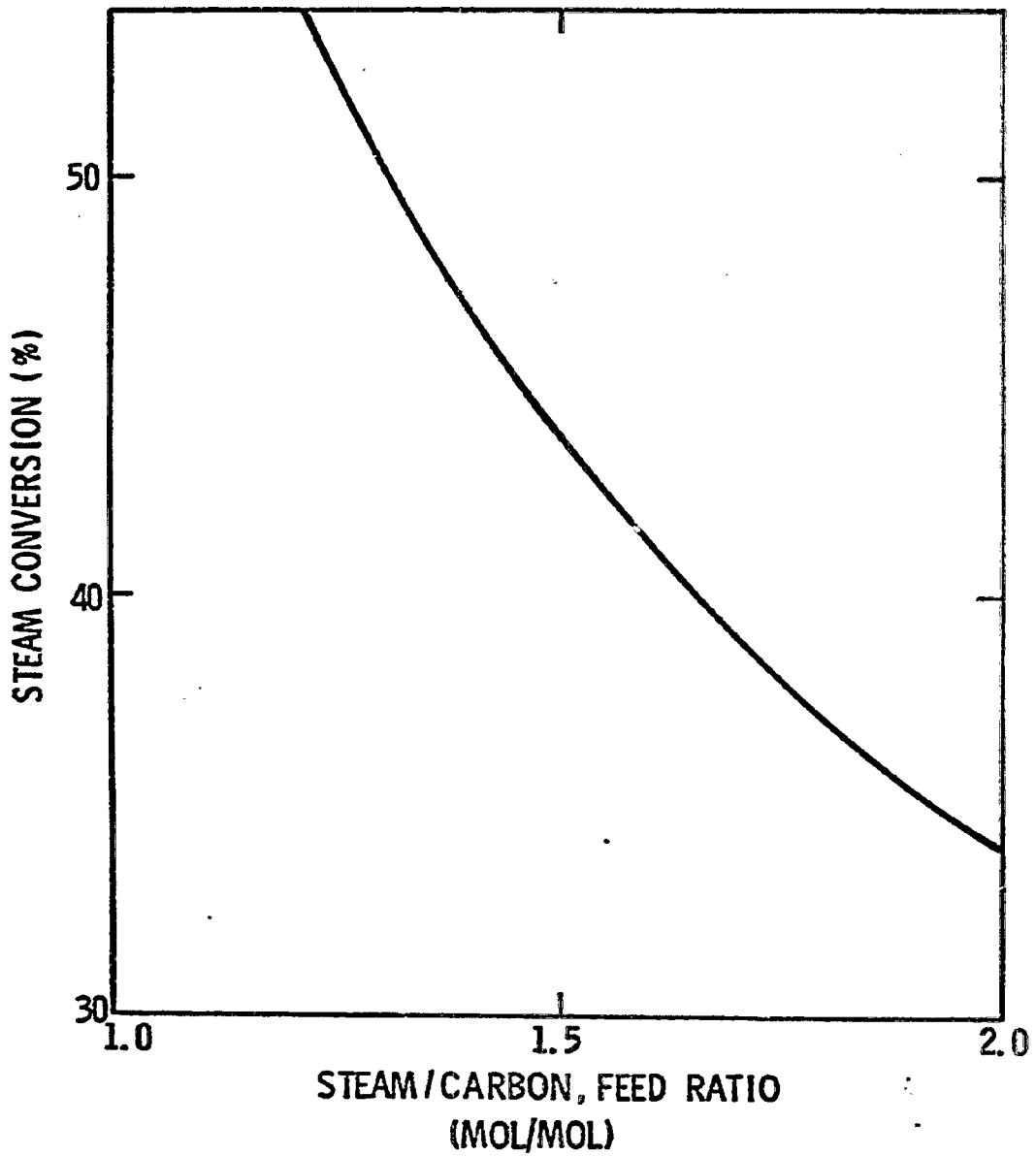


FIGURE 3.1-13
METHANE PRODUCED DEPENDS ON FEED RATIO
MODEL SIMULATION OF PDU

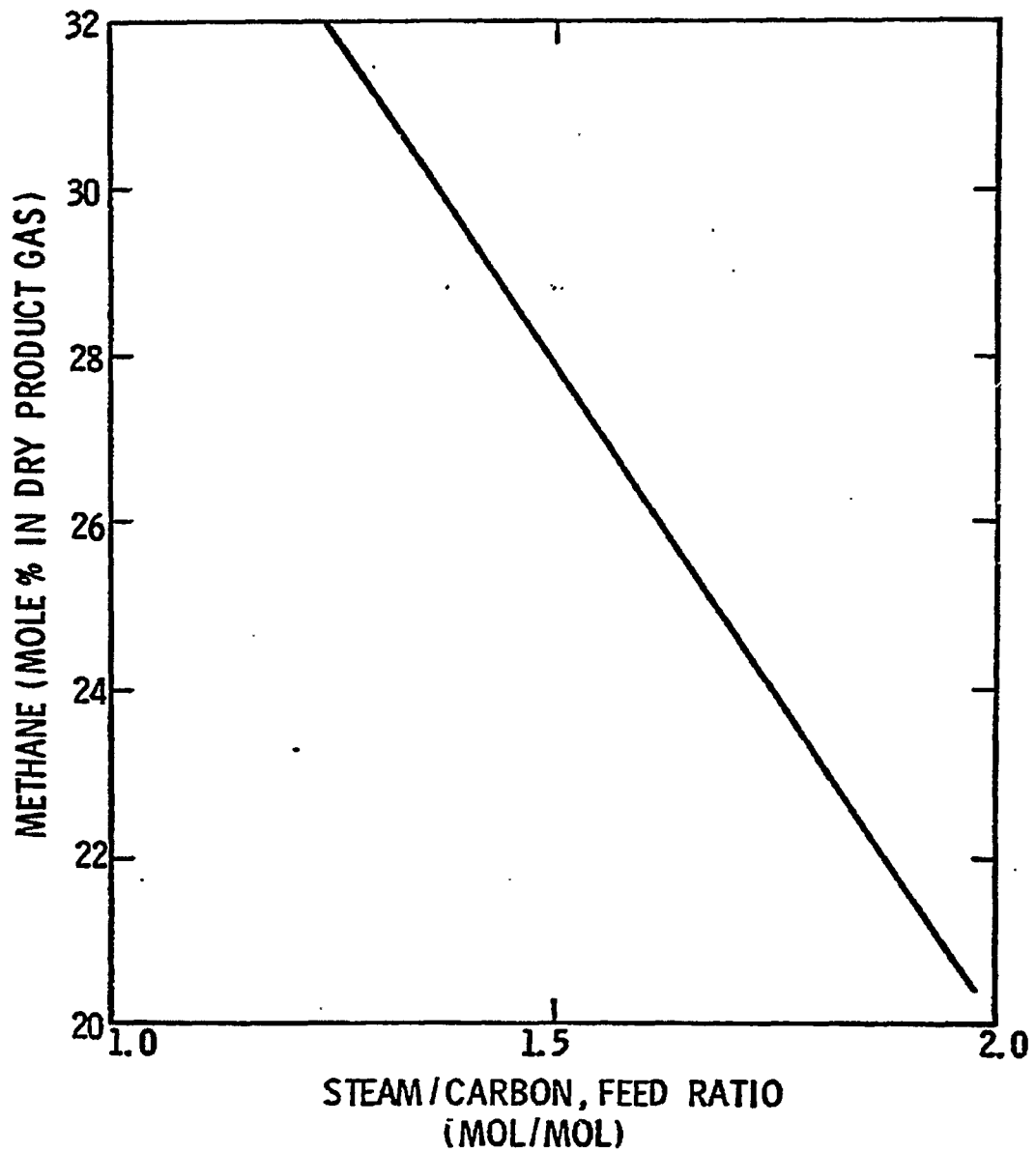
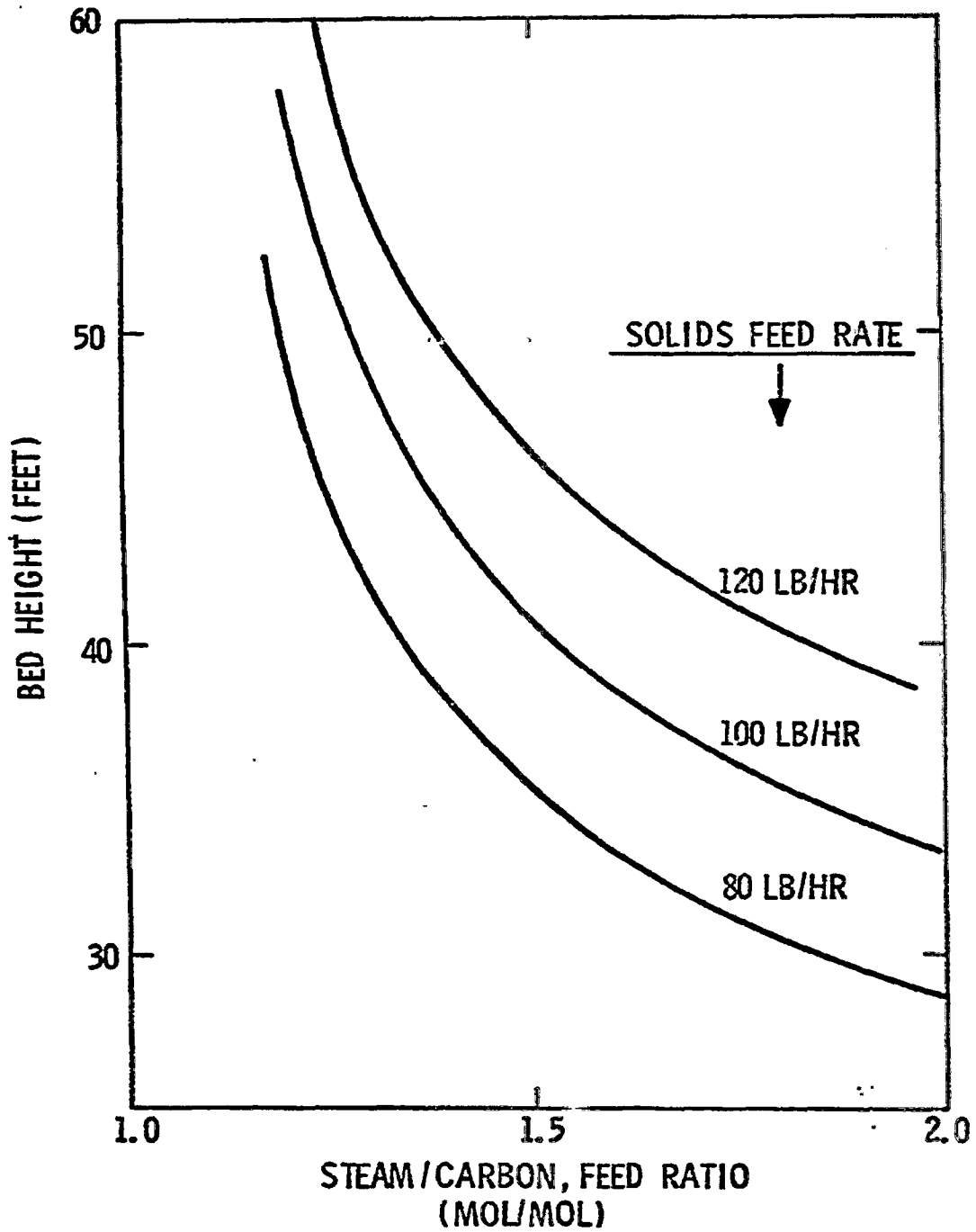


FIGURE 3.1-14

BED HEIGHT REQUIREMENTS
MODEL SIMULATION OF PDU



The ratio of the synthesis gas to be recycled to the CH₄ produced increases linearly with the H₂O/C ratio under syngas balanced conditions as shown in Figure 3.1-15. Of the total synthesis gas to be recycled, the molar ratio of H₂/CO required under the syngas balanced conditions increases with an increasing H₂O/C ratio as shown in Figure 3.1-16. Thus, at higher H₂O/C molar feed ratios, the refined syngas would be increasingly H₂ rich.

In a separate study, the effect of system pressure on CH₄ production was examined. Comparing two cases at 500 and 265 psia, with all other parameters remaining constant, the higher pressure was found to favor higher methane formation as shown in Figure 3.1-17.

This series of computations demonstrated that the model is useful in providing insight and guidance to pilot plant operations.

Demonstration Run Guidance

The CCG reactor model was used to assist in the setting of the PDU operating conditions for the demonstration run. It was decided that the PDU performance should satisfy the following target conditions:

Carbon conversion :	85%
Steam conversion:	35%
CH ₄ in dry product gas:	25%
Syngas balance:	80%

On the basis of 85% carbon conversion and 100% syngas balance, the performance of the gasifier as predicted by the model is shown in Figures 3.1-18 to 3.1-20. Figure 3.1-18 shows that both the steam conversion and the CH₄ concentration in dry product gas will decrease as the molar ratio of steam-to-carbon in feed increases. At a H₂O/C ratio of 1.5, for example, steam conversion is at about 40% and CH₄ concentration at 28%. Figure 3.1-19 shows that under syngas balanced conditions, the total moles of recycle syngas increase with the H₂O/C ratio. Also the H₂-to-CO ratio in the recycled gas increases with the H₂O/C ratio. Again, at a H₂O/C of 1.5, the H₂-to-CO ratio is about 4 and the syngas to CH₄ ratio is about 1.7. Figure 3.1-20 shows that the required solids nominal residence time decreases with increasing H₂O/C ratio. About 10 hours of solids nominal residence time will be needed at a H₂O/C of 1.5.

The PDU coal feed system uses syngas to transport coal into the gasifier. The amount of syngas required increases with increasing coal feed rate. This requirement causes difficulty in achieving the targeted 80% syngas balance. The model was used to provide some insight into this area. Figure 3.1-21 shows that at a proposed H₂O/C ratio of 1.43, the amount of syngas required for 100% syngas balance is about 1800 SCFH. A syngas flow rate of 2800 SCFH will give 80% syngas balance. If higher syngas flow rates must be used for coal feeding purposes, Figure 3.1-22 shows that the H₂O/C ratio should be increased to enhance syngas balance for any given syngas flow rate. These higher H₂O/C ratios result in decreased methane content of the product gas.

FIGURE 3.1-15
RECYCLE REQUIREMENT CHANGES WITH FEED RATIO
MODEL SIMULATION OF PDU

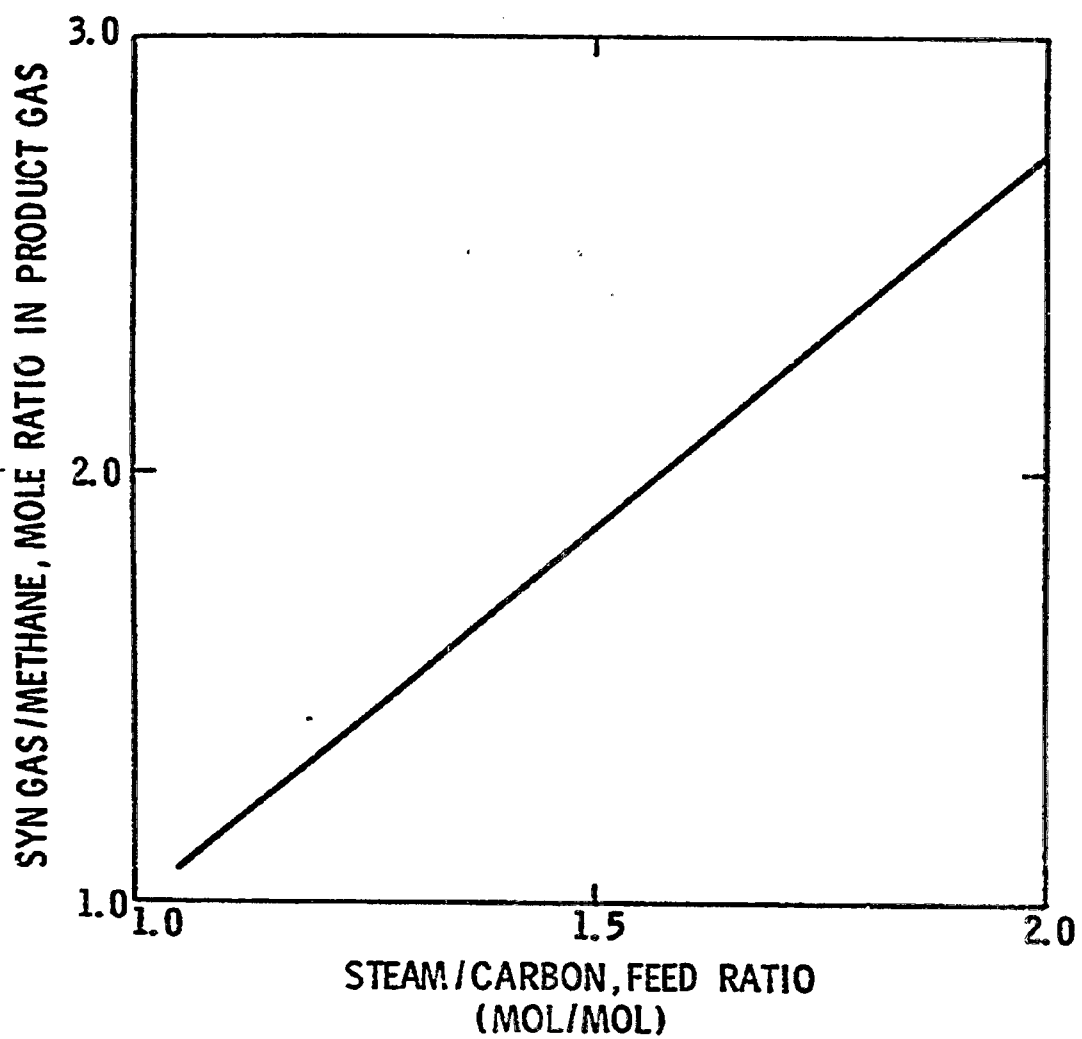


FIGURE 3.1-16

COMPOSITION OF SYN GAS CHANGES WITH FEED RATIO
MODEL SIMULATION OF PDU

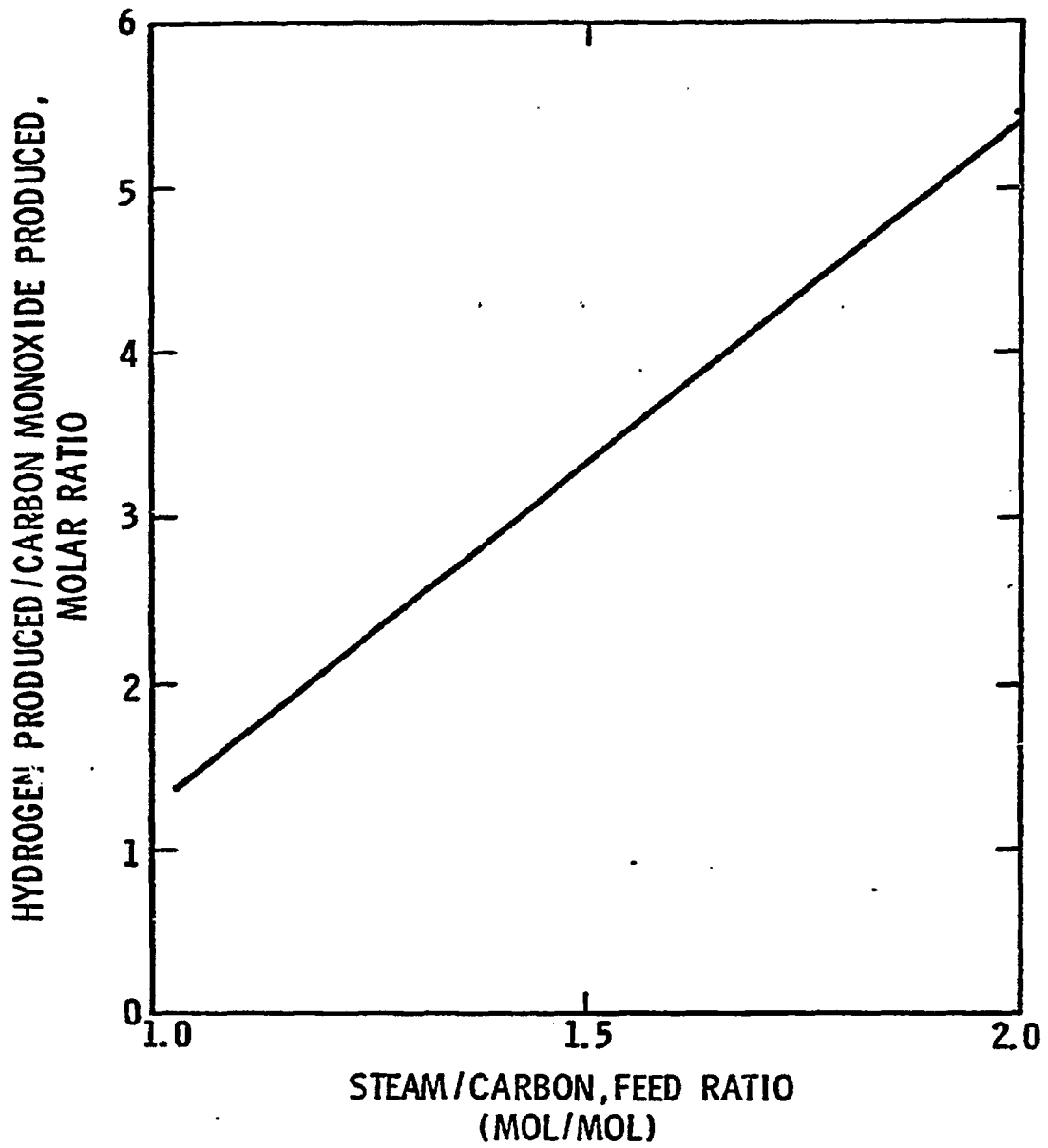


FIGURE 3.1-17
EFFECT OF PRESSURE ON CH₄ FORMATION
MODEL SIMULATION OF PDU

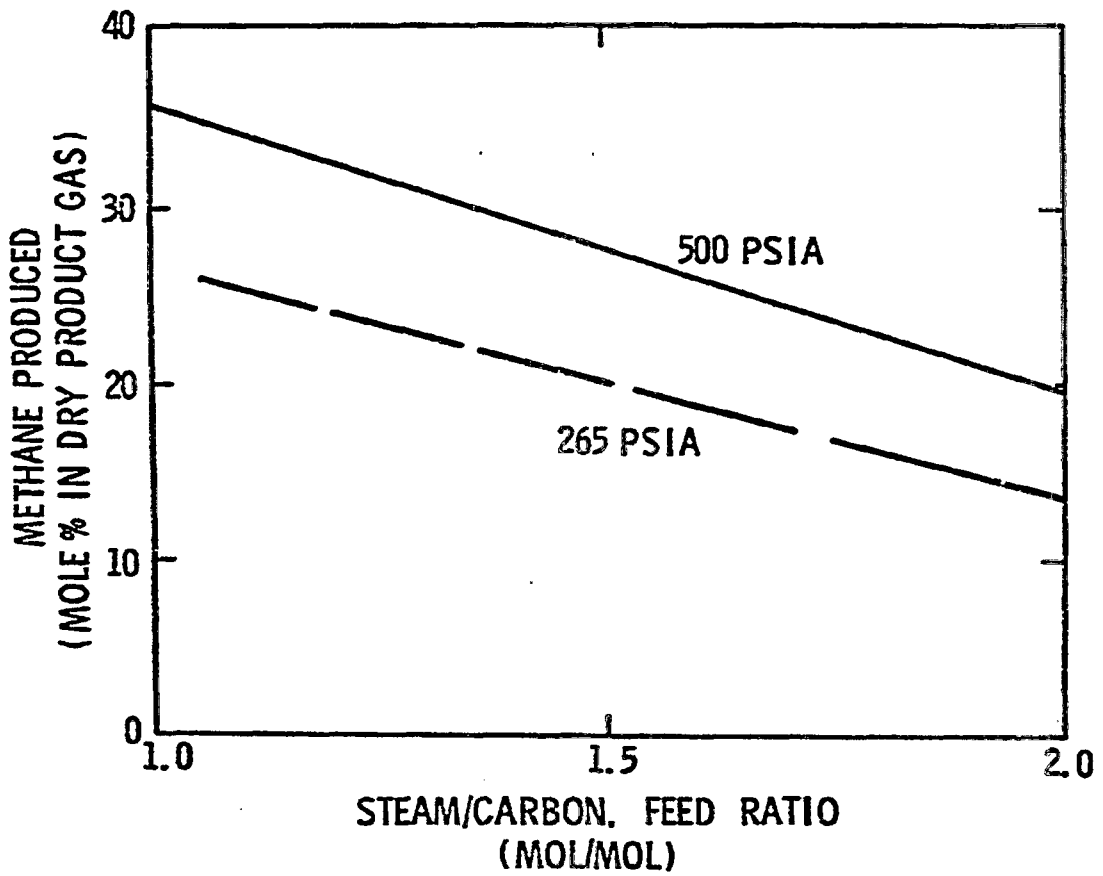


FIGURE 3.1-18
STEAM CONVERSION AND CH₄ CONCENTRATION
AT 85% CARBON CONVERSION

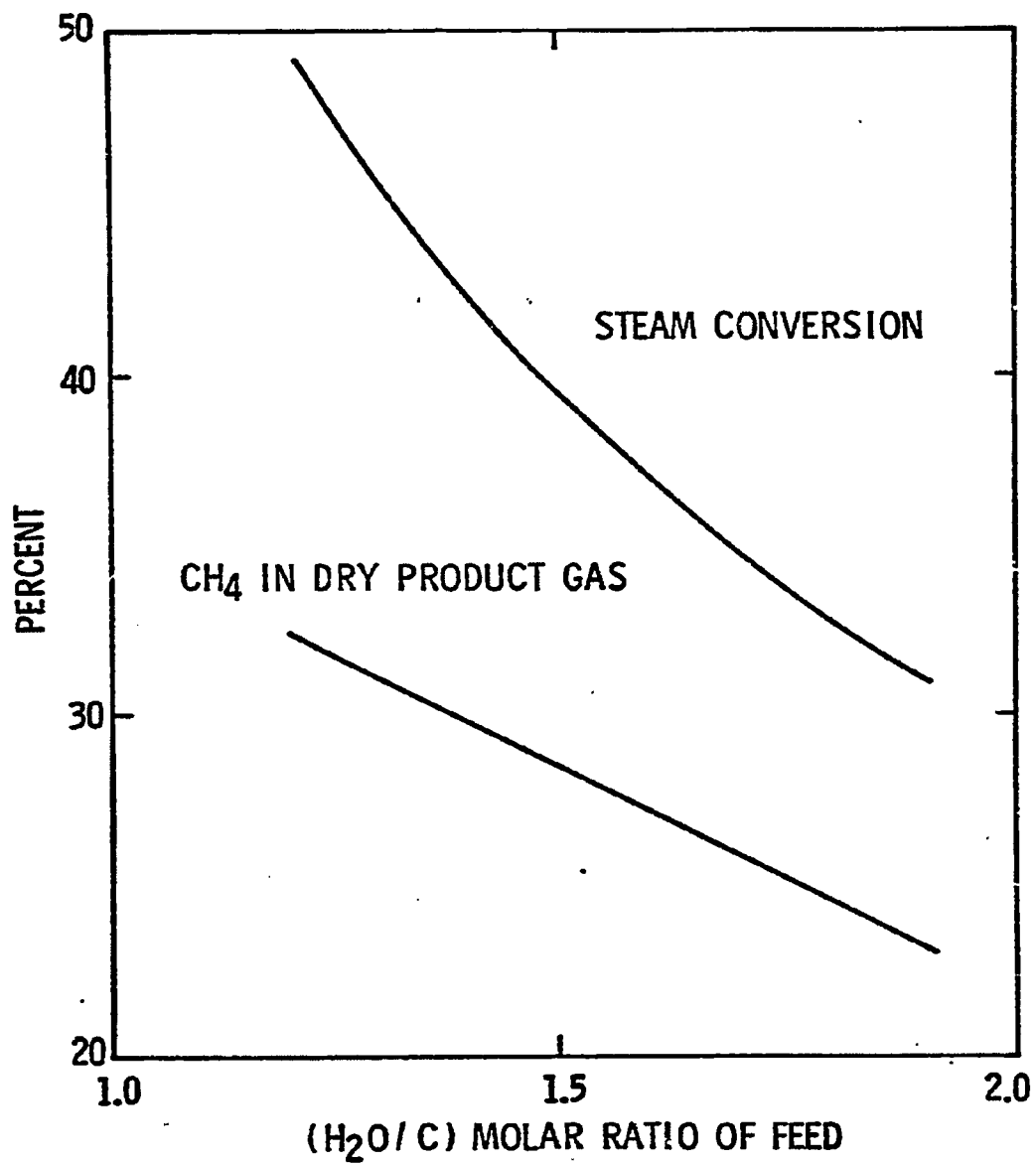


FIGURE 3.1-19
SYN GAS RECYCLE AT 85%
CARBON CONVERSION

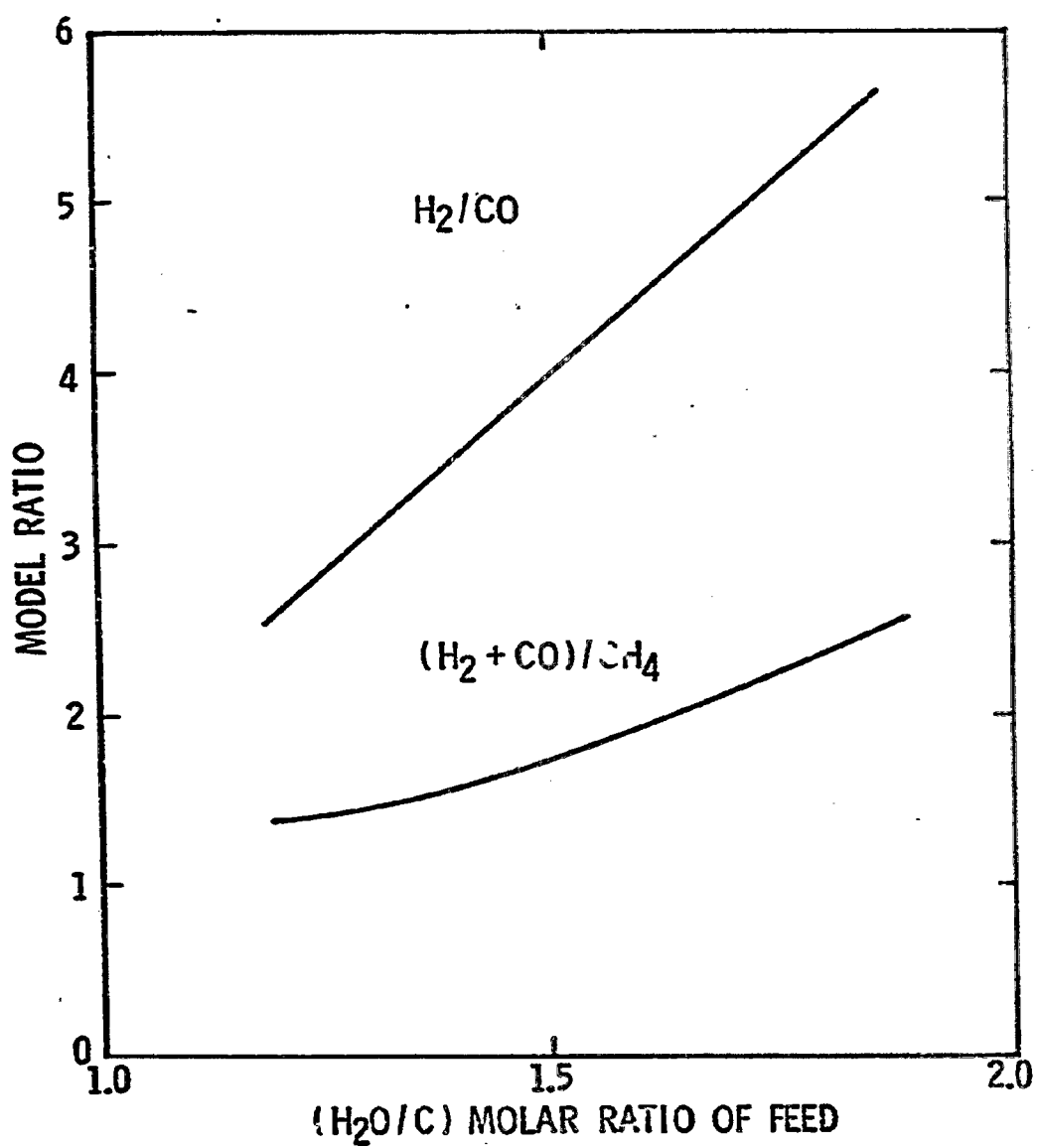


FIGURE 3.1-20
SOLIDS RESIDENCE TIME FOR
85% CARBON CONVERSION

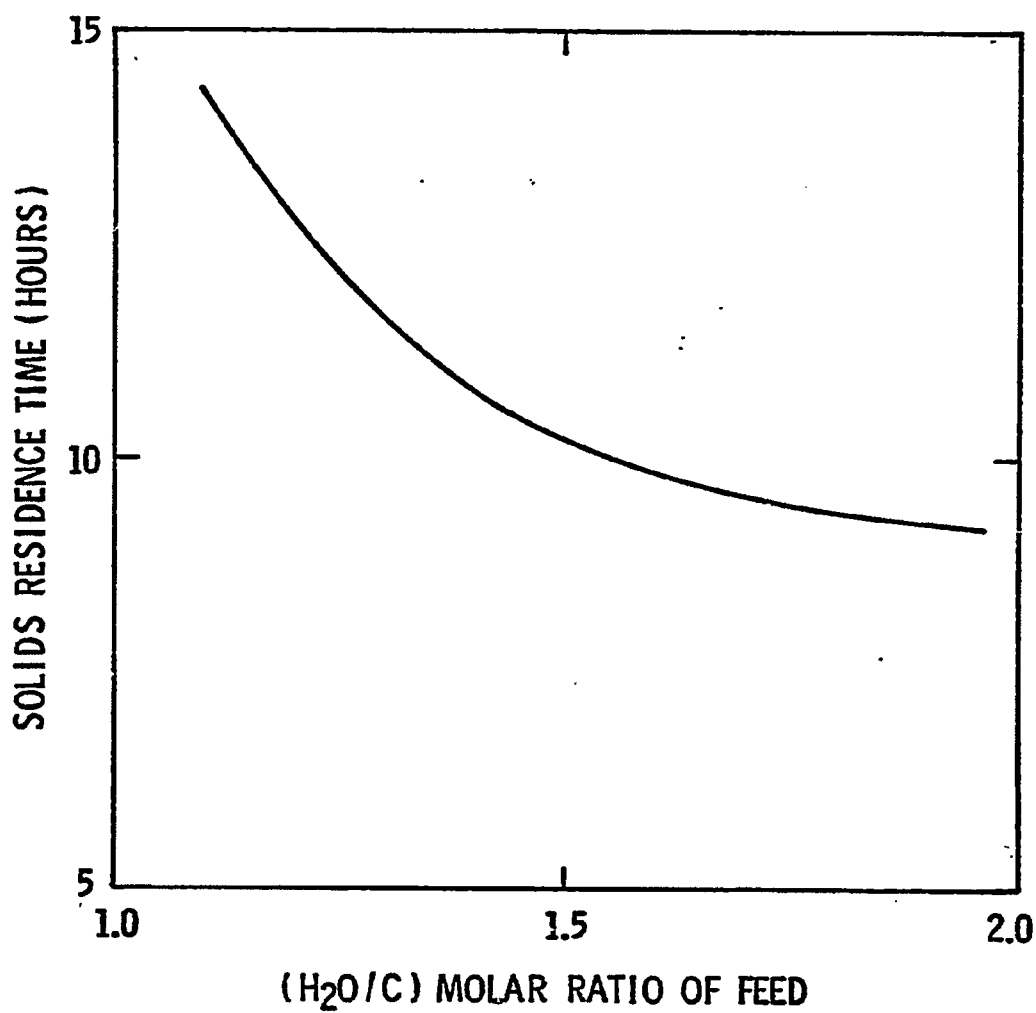


FIGURE 3.1-21
SYN GAS BALANCE AS A FUNCTION OF FLOW RATE

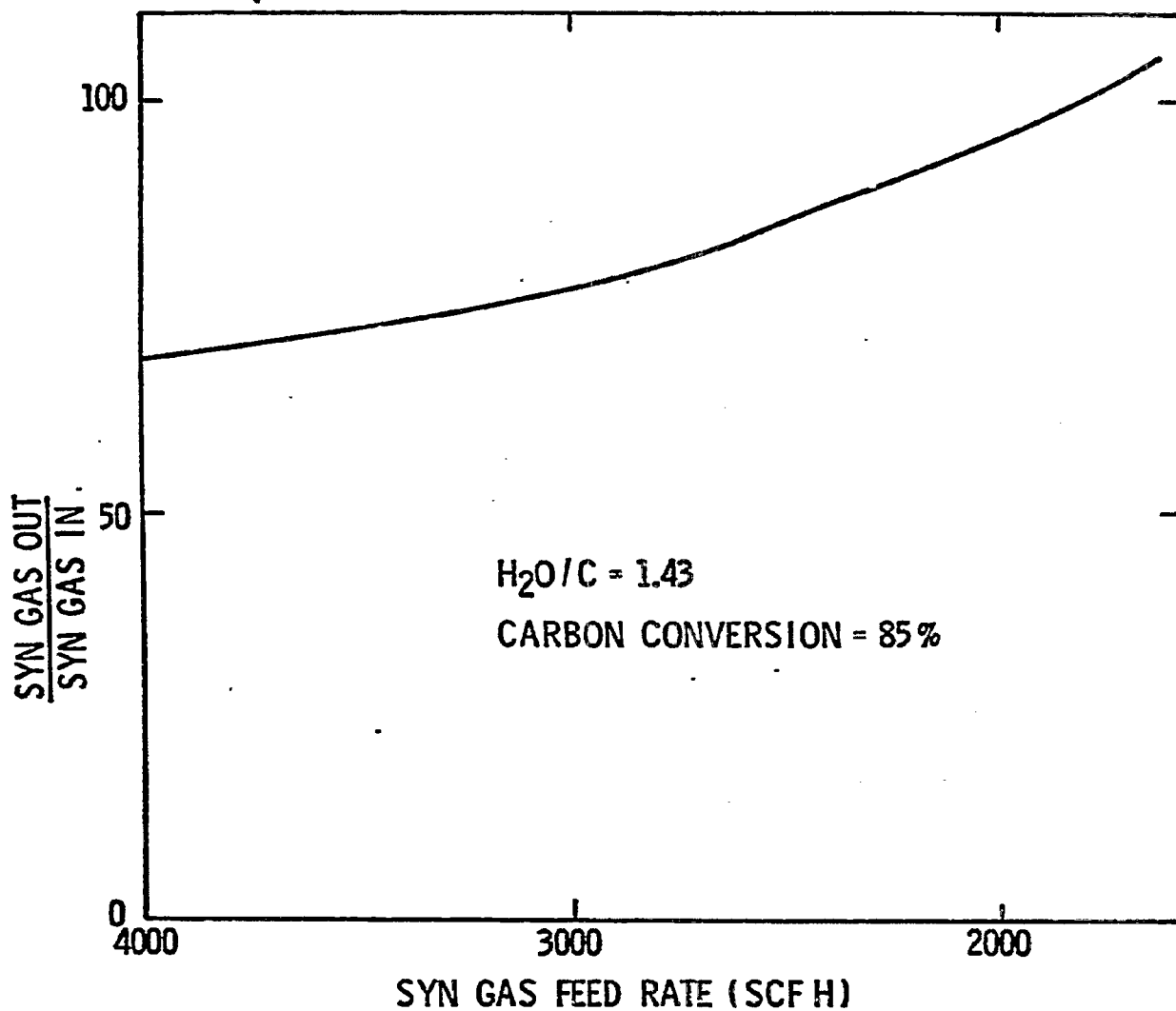
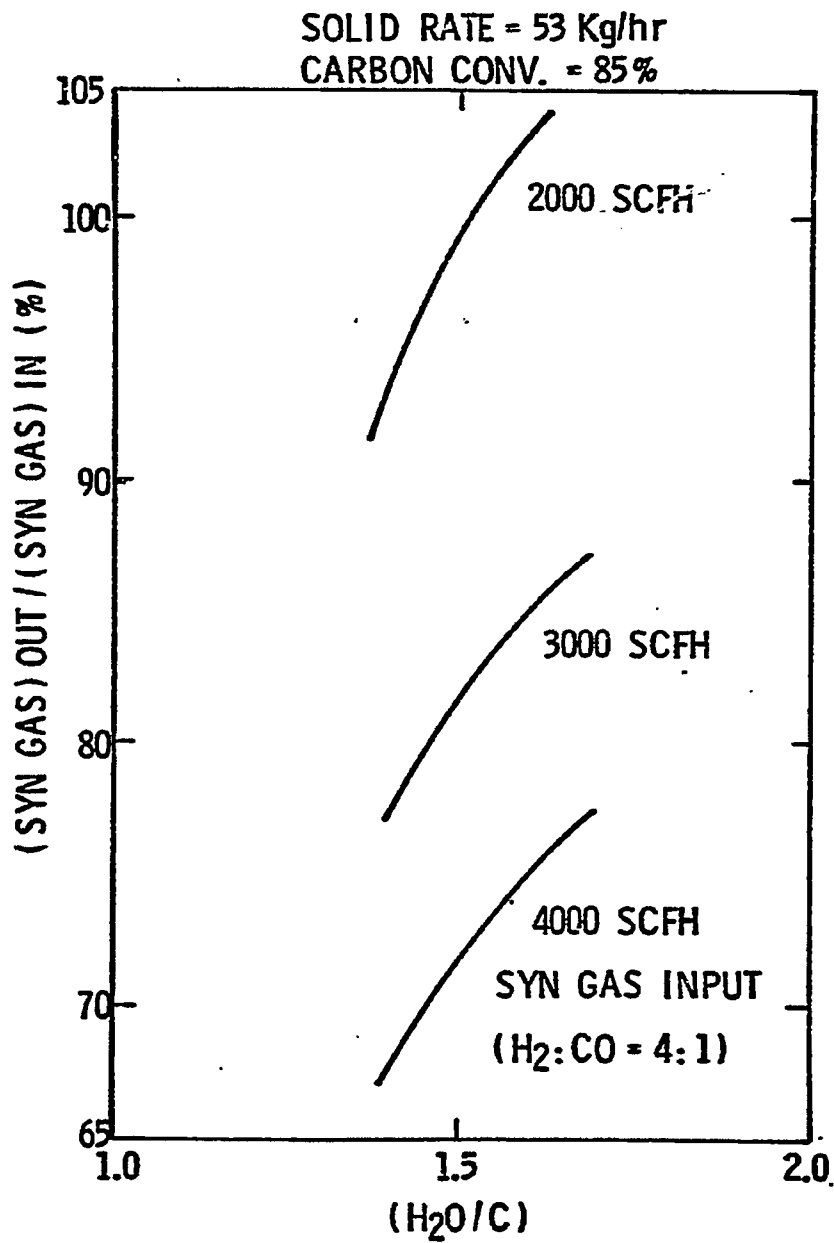


FIGURE 3.1-22
SYN GAS BALANCE AS A FUNCTION OF H₂O/C RATIO



Model Validation

Validation of the gasifier model is an ongoing task. The most convincing test to date has been to compare the 14 material balance periods from the demonstration run with the model predictions. For this set of model runs, the actual feed flow rates and the actual carbon conversion were used as inputs to the model. The model was then used to predict the bed height required to achieve the observed carbon conversion.

Table 3.1-4 and Figures 3.1-23 and 3.1-24 contain the predicted and observed bed heights and methane yields for the 14 demonstration run material balance periods. For completeness, they also contain 17 FBG yield periods from the predevelopment contract work and the 7 other PDU yield periods. In most cases, the predicted and observed bed height agree within +10%. The low density (<10 lbs/ft³) runs are notable exceptions. In these cases, the model predicts that a very tall bed would be required to achieve the observed carbon conversion; whereas, in the pilot unit a very tall bed was not necessary.

Table 3.1-4

SIMULATION OF PILOT PLANT OPERATIONS

	Run Number	Gasifier Bed Height (feet)		Methane, % of Dry, N ₂ - Free Product Gas		
		Actual	Predicted	Predicted	Actual	
FBG	YP-202	31.5	23.7	5.3	10.1	
	YP-203	35.2	32.3	6.5	11.6	
100 psig	YP-204	29.7	34.3	10.8	11.8	
	YP-205	29.1	40.4	8.3	10.9	
	YP-206	34.9	38.7	7.4	11.0	
	YP-207	34.2	34.1	8.2	11.2	
	YP-208	32.1	54.0	10.9	11.4	
	YP-209	34.7	39.8	5.7	7.8	
	YP-210	31.2	31.2	5.4	7.4	
	YP-211	31.8	27.0	10.3	12.5	
	YP-212	38.8	40.3	9.2	13.0	
	YP-213	36.6	34.0	10.2	11.5	
	YP-214	30.7	28.2	9.2	9.7	
	YP-215	36.6	35.4	9.2	8.9	
	YP-216	32.5	27.1	6.7	7.8	
	YP-218	35.2	28.3	7.3	9.5	
	YP-219	29.9	33.2	7.5	8.2	
	PDU	YP-1	46.5	43.8	16.6	22.2
		YP-2	56.0	48.7	16.5	18.5
YP-3		57.8	72.4	13.9	18.6	
265 psia	YP-4	54.8	88.2	17.0	14.1	
	YP-5	59.1	73.8	17.0	18.8	
	YP-6	64.4	79.2	17.9	18.6	
	YP-7	52.2	70.7	17.2	19.5	
PDU	YP-8	55.0	49.9	27.4	26.9	
	YP-9	47.1	41.9	25.4	25.0	
500 psia	MB-54	51.2	51.5	19.4	19.9	
	MB-55	48.7	48.3	21.4	19.9	
	MB-56	48.7	50.2	21.9	18.1	
	MB-57	55.2	54.6	24.4	22.7	
	MB-58	49.7	55.5	25.8	25.0	
	MB-59	52.9	52.7	25.8	22.2	
	MB-60	57.2	48.1	22.7	21.3	
	MB-61	58.5	53.6	22.6	20.5	
	MB-62	57.2	62.1	23.8	19.9	
	MB-63	57.2	54.9	21.8	19.4	
	MB-64	58.5	59.6	22.9	19.2	
	MB-65	55.2	81.7	22.2	17.9	
	ME-66	48.7	60.8	17.4	15.2	
	MB-67	58.5	69.3	23.9	20.6	

FIGURE 3.1 - 23

PARITY PLOT OF MODEL WITH PILOT PLANT DATA
(BED HEIGHT.)LEGEND

- ▽ FBG 100 PSI
- ◇ PDU 265 PSI
- PDU 500 PSI

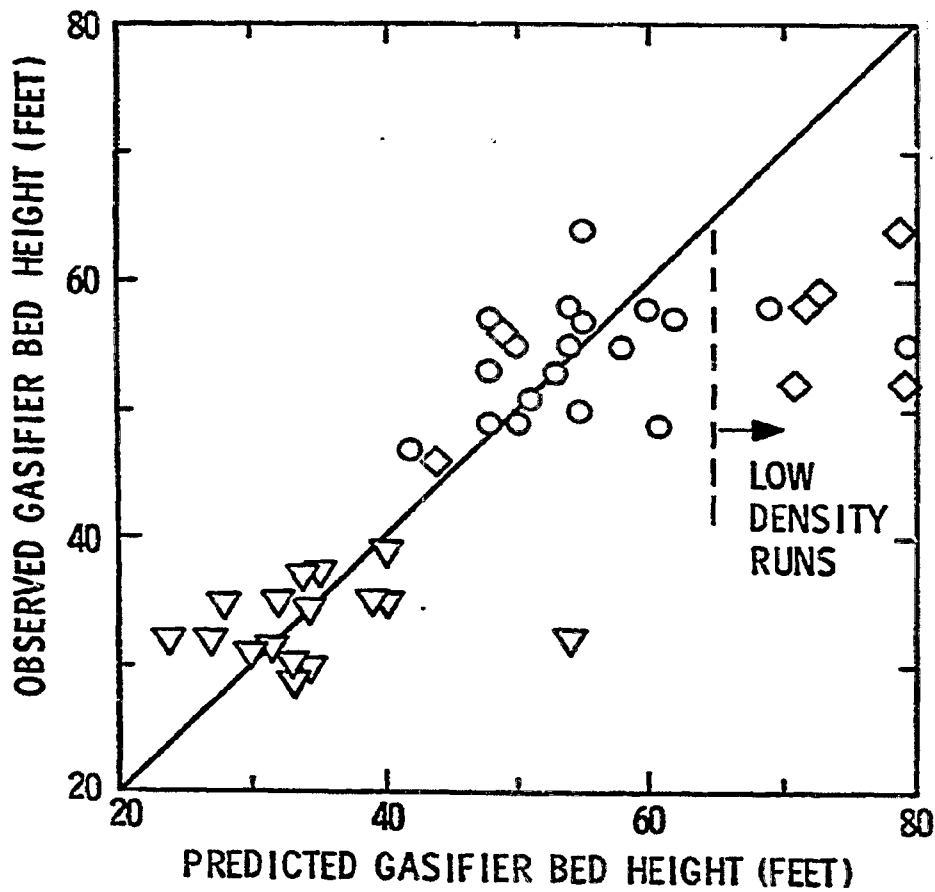
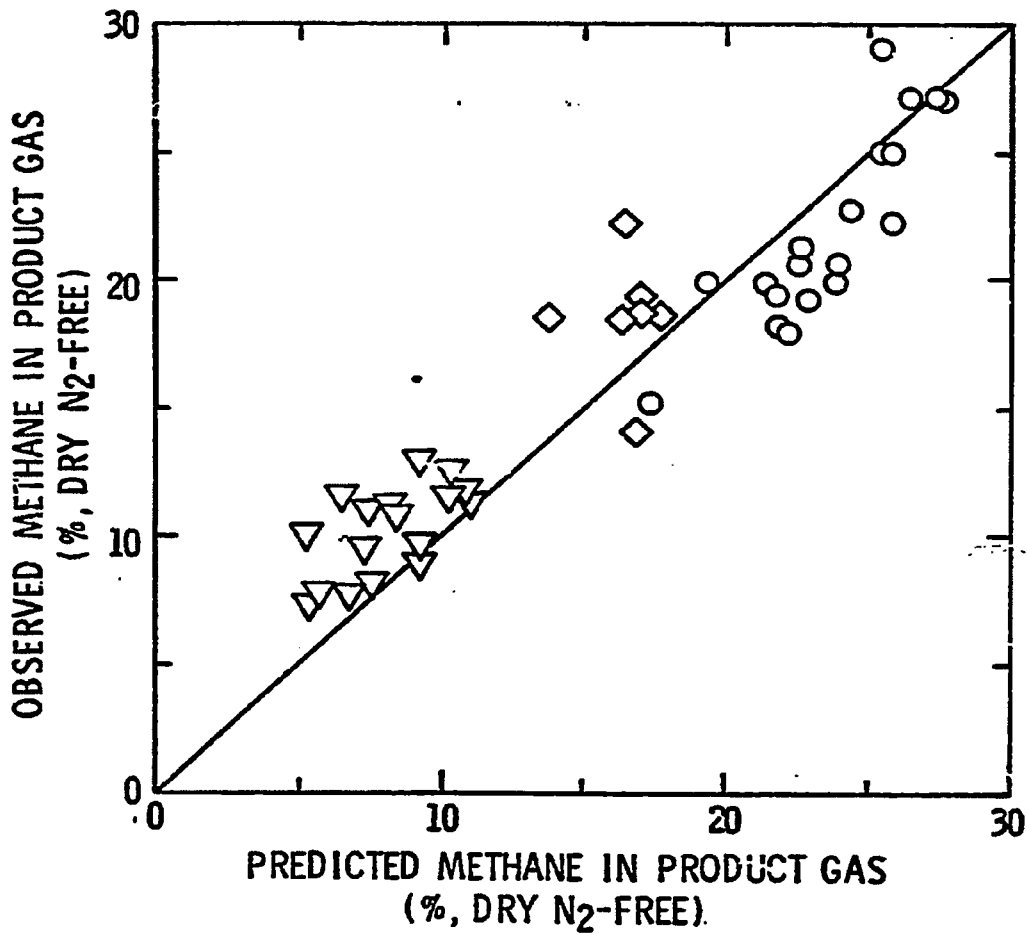


FIGURE 3.1 - 24
PARITY PLOT OF MODEL WITH PILOT PLANT DATA
(METHANE)

LEGEND

- ▽ FBG 100 PSI
- ◇ PDU 265 PSI
- PDU 500 PSI



References:

1. J. M. Eakman, et al., "Gasifier Operation and Modeling in Exxon CCG Process", presented at 72nd Annual Meeting of AIChE, Nov., 1979.
2. D. Kunii and O. Levenspiel, Fluidization Engineering, Wiley, 1969.
3. J. F. Davidson and D. Harrison (Ed.), Fluidization, Academic Press, 1971, Chap. 5.
4. C. J. Vadovic and J. M. Eakman, "Kinetics of Potassium Catalyzed Gasification", presented at 176th National Meeting of ACS, Miami, September, 1978.
5. D. Geldart, Powder Technology, 7, (1973), p. 285.
6. D. Geldart and A. R. Abrahamsen, Powder Technology, 19, (1978), p. 133.
7. J. F. Richardson and W. N. Zaki, Trans. Inst. Chem. Eng., 32, (1954), p. 35.
8. D. Geldart, Powder Tech., 6, (1972), p. 201
9. P. N. Rowe, Chem. Eng. Science, 31, (1976), p. 285.
10. Darton, et al., Trans. Inst. Chem. Eng. 55, (1977), p. 274.
11. Harrison, et al., Trans. Inst. Chem. Eng. 39, (1961), p. 202.
12. R. Clift, et al., Ind. Eng. Chem. Fund. 13, (1974), p. 45.

3.2 On-Line Data Acquisition and Off-Line Data Reduction and Reconciliation

On-Line Data Acquisition

The purpose of the on-line data acquisition and reduction system is to monitor the PDU pilot plant operation and to provide evaluation of operating data. Design of the system is shown schematically in Figures 3.2-1 and 3.2-2. Analog signals from sensors on the unit, such as pressure transmitters, weigh cells, and thermocouples are converted to digital form in the analog/digital converter. This data is transferred to the memory of a mini-computer. The memory contains software necessary for alarming, logging, and operator interface functions for the Process Development Unit (PDU). Data are stored on disc for future display on cathode ray tubes (CRT) or printers, and for long term storage on tapes.

Routine Data Processing and Acquisition

Routine data processing includes scanning of all digital and analog process data variables at intervals ranging from 20 seconds to one hour and conversion of digital and analog data to engineering units. The types and approximate number of process variables are tabulated below.

<u>Type of Measurement</u>	<u>Number of Measurement Points</u>
Temperatures	400
Flows	30
Pressures	60
Gas Analyses	100
Weights	<u>10</u>
TOTAL	600

During unit operations, values of all process variables are instantly available to operators in the form of a digital readout accessed by a keyboard in the control room. The computer has been programmed to provide process operation profiles displayed on the operator request CRT screens.

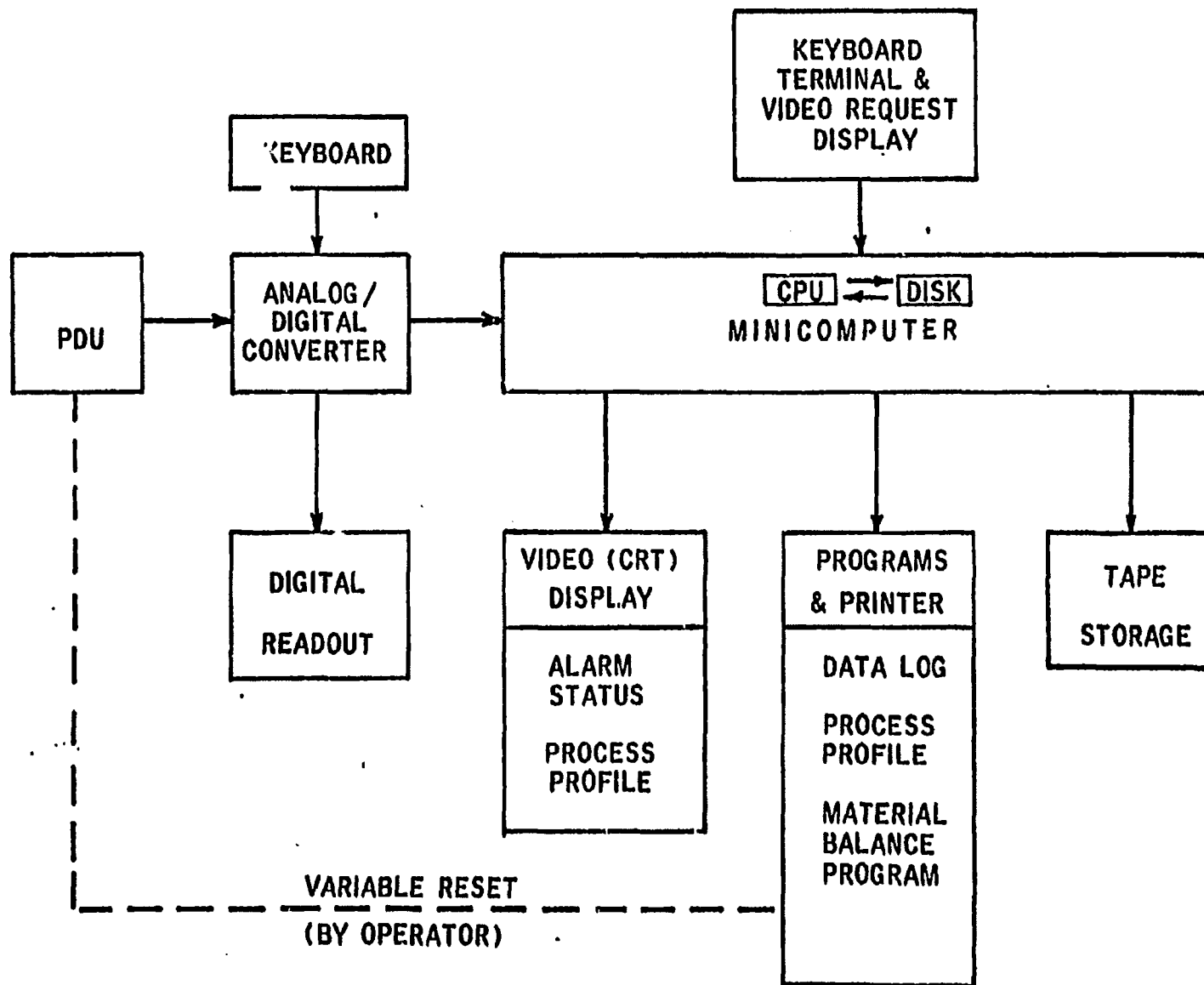
Alarm Processing and Checking

The system can determine if process variables go above or below their maximum or minimum allowed values. Variable alarms result in a printed message displayed on alarm CRT's and printers. For most variable alarms, the system also updates the variable's status. The displays on alarm CRT's are updated once a minute with current alarm information.

Data Logging

Three different log formats are available. An hourly log consists of all the values for a shift through the last hour for each variable. A period log consists of averages for a specified period for each variable. A demand log consists of the current value and previous hour average, maximum, and minimum for each variable. Both the demand and period average logs can be requested as desired.

FIGURE 3.2-2
PDU ON-LINE DATA ACQUISITION SYSTEM



201

On-line Data Evaluation

On-line data evaluation is accomplished by a material balance program stored in the memory of the computer. This program input consists of 44 measurements such as temperatures, pressures, and flows. Four material balances (overall, hydrogen, oxygen, and syngas) as well as average unit conditions are computed and printed. This program not only provides guidance on conditions required to achieve a desired conversion but also aids in locating operating problems.

Off-line Data Reduction and Reconciliation

The purpose of off-line data reduction and reconciliation is to provide consistent and reliable data for use in correlations, commercial plant study designs, and kinetic model development. Plant operations data have inaccuracies due to random instrumentation errors and inability to measure some quantities. Furthermore, some data may be in error as a result of faulty or incorrectly calibrated meters. As a result, raw operations data may not exactly satisfy material balance constraints. Use of these inconsistent and erroneous data for feasibility studies and decision making may lead to incorrect conclusions. To resolve the inconsistencies in the pilot plant data, a data reconciliation technique is used. Data reconciliation consists of adjusting the measured operations data based on estimated tolerances assigned to each variable; that is, the most reliable data will be changed least and the least reliable data the most in order to satisfy the material balance constraints. In this way, random instrumentation errors are corrected, unmeasured quantities are determined, and faulty measurements are isolated and flagged for correction.

The mathematical formulation of the data reconciliation problem consists of:

$$\text{minimize: } f(R) = \sum_i \frac{(M_i - R_i)^2}{\sigma_i^2} \quad \begin{array}{l} i = 1, \dots, \text{NVAR} \\ j = 1, \dots, \text{NCØN} \end{array}$$

$$\text{subject to: } E_j(R) = 0$$

where: M_i = Measured value of variable i
 R_i = Reconciled value of i
 σ_i = Standard deviation of the i th measurement
 E_j = Set of nonlinear equations representing the physical relationship among the variables
NVAR = Number of variables
NCØN = Number of constraints

Standard deviation is defined in terms of reliability for each measured variable as follows:

$$\sigma_i = M_i \cdot \text{rel}_i / 200$$

Reliability (rel_i) is an estimate of the quality of individual data points based upon the user's experience. For example, a reliability of 10% implies that if a measuring device is functioning properly, it will measure to within $\pm 10\%$ of the true value 95% of the time (i.e., two-standard deviations). Thus, a small numerical value for reliability indicates the measured value is of high quality.

The objective function used in reconciliation represents the sum of the deviations of the reconciled variables from the measure values. These deviations are weighted by the user's estimate of the reliability of the measurements. During the iterative minimization of the objective function, the algorithm attempts to keep reconciled values for reliable measurements close to measured values. The constraints which describe physical relationships of process variables (such as material balances) must be satisfied during minimization of the objective function. The algorithm is shown schematically in Figure 3.2-3.

Two versions of the reconciliation program are used. The first, referred to as intermediate reconciliation, appropriate temperatures, pressures, and flow rates as well as carbon, hydrogen, potassium and ash values for feed coal plus catalyst (FC), gasifier mid char (GMC), gasifier bottom char (GB) and entrained char captured in the gasifier product gas filters (GF). Results from this data work-up are summarized for all 67 material balance periods defined between December 1979 and April 1981 (Table 3.2-1). The second version, referred to as full reconciliation and used for Yield Periods, requires all of the data input for the immediate reconciliation as well as additional temperatures, pressures, elemental analyses, and particle size analysis. Multiple samples are chosen for analysis and eight ash elements are analyzed and balanced. Results from this work-up for nine Yield Periods defined between May 1980 and November 1980 are given in the Appendix. Also given in the Appendix are intermediate reconciliation data for four additional Yield Periods for which full reconciliation is not yet available. Included for each material balance period summarized in Table 3.2-1 are feed and output rates, conversions, fluid-bed properties, syngas balances and selected kinetic parameters. These periods cover a broad range of operating conditions, including the following:

Gasifier Coal Feed Rate	52-132 lbs/hr
Gasifier Pressure	116-500 psia
Gasifier Temperature	1213-1297°F
Fluid Bed Density	5-32 lbs/ft ³
Carbon Conversion	30-95%
Steam Conversion	17-44%

FIGURE 3.2-3
DATA RECONCILIATION

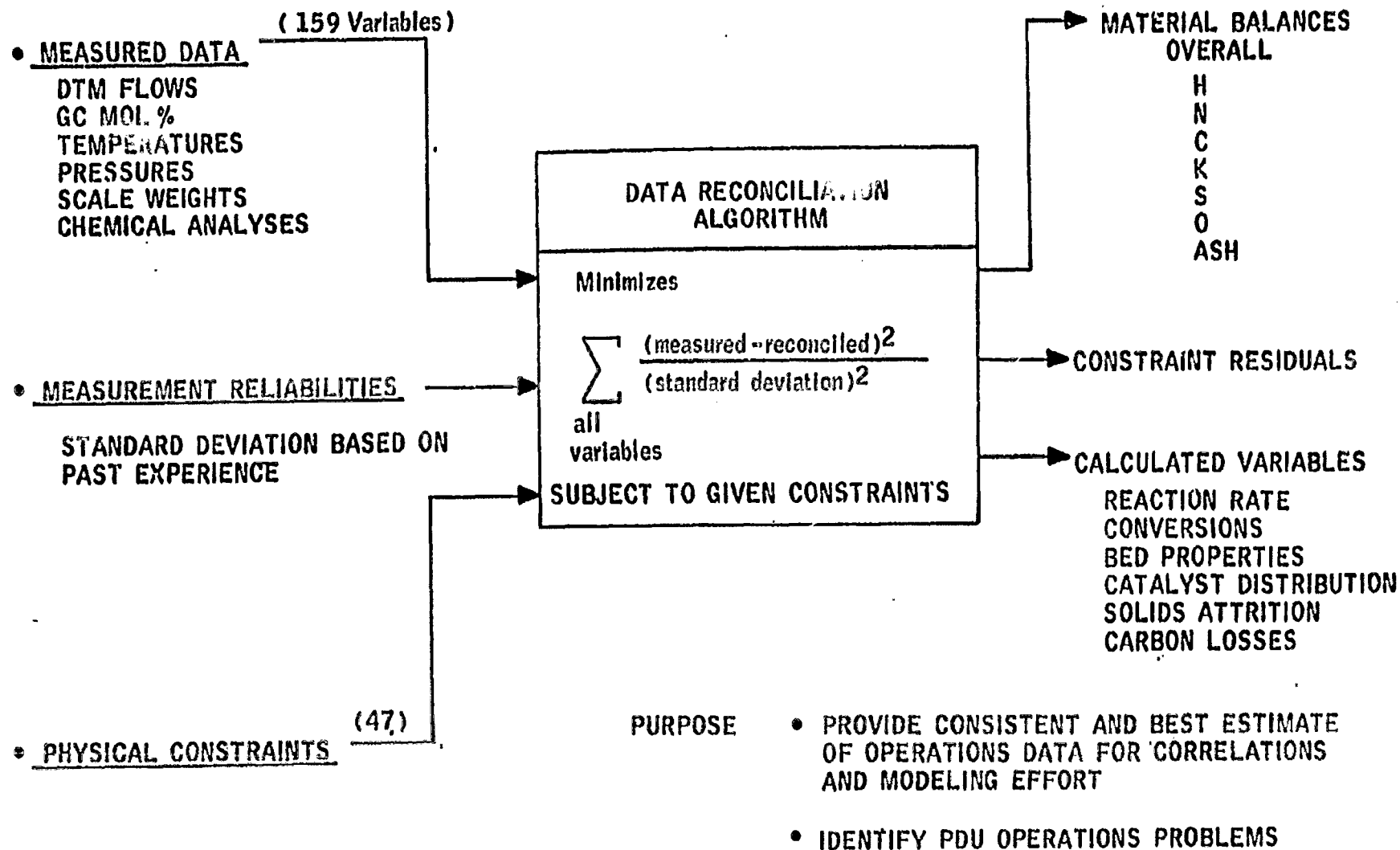


Table 2.2 (cont'd)

Item	YF-4					YF-5					YF-6					YF-7					YF-8					YF-9				
	26	27	28	29	30	31	32	33	34	35	36	37	38	39	40	41	42	43	44	45	46	47	48	49	50	51	52	53	54	55
Run Time (hrs)	15-25-00	16-17-00	18-19-00	20-21-00	22-23-00	24-25-00	26-27-00	28-29-00	30-31-00	32-33-00	34-35-00	36-37-00	38-39-00	40-41-00	42-43-00	44-45-00	46-47-00	48-49-00	50-51-00	52-53-00	54-55-00	56-57-00	58-59-00	60-61-00	62-63-00	64-65-00	66-67-00	68-69-00	70-71-00	72-73-00
Duration (hrs)	24	24	24	24	24	24	24	24	24	24	24	24	24	24	24	24	24	24	24	24	24	24	24	24	24	24	24	24	24	24
Gasifier Temp (°F)	1258	1272	1282	1284	1284	1280	1272	1264	1258	1250	1242	1234	1226	1218	1210	1202	1194	1186	1178	1170	1162	1154	1146	1138	1130	1122	1114	1106	1098	1090
Gasifier Pressure (psia)	279	265	267	264	265	265	267	275	287	307	327	347	367	387	407	427	447	467	487	507	527	547	567	587	607	627	647	667	687	707
Richard Pressure (psia)	245	247	249	247	247	247	247	247	247	247	247	247	247	247	247	247	247	247	247	247	247	247	247	247	247	247	247	247	247	247
Mode of Operation	Batch	Coal																												
Top of Bed (ft)	1248	1290	1285	1283	1284	1280	1272	1264	1258	1250	1242	1234	1226	1218	1210	1202	1194	1186	1178	1170	1162	1154	1146	1138	1130	1122	1114	1106	1098	1090
Input (lb/hr)	217.06	265	259.31	249.37	248.69	232.63	241.87	242.6	239.03	208.4	199.22	199.2	204.9	202.2	212.8	210.8	213.4	213.4	213.4	213.4	213.4	213.4	213.4	213.4	213.4	213.4	213.4	213.4	213.4	213.4
Coal	55.37	74.46	77.96	69.81	73.76	68.92	69.87	71.9	78.32	56.04	56.27	70.0	99.5	97.7	99.8	97.0	98.0	98.0	98.0	98.0	98.0	98.0	98.0	98.0	98.0	98.0	98.0	98.0	98.0	98.0
Steam	108.82	119.9	115.10	115.13	111.23	114.59	109.17	107.14	104.89	97.00	91.87	93.6	144.8	145.7	147.0	149.3	148.1	147.8	147.8	147.8	147.8	147.8	147.8	147.8	147.8	147.8	147.8	147.8	147.8	147.8
Syn Gas	53.57	77.64	66.25	66.43	63.70	60.50	62.94	64.1	57.9	55.6	52.07	33.6	60.0	59.1	64.0	63.0	63.0	63.0	63.0	63.0	63.0	63.0	63.0	63.0	63.0	63.0	63.0	63.0	63.0	63.0
Output (lb/hr)	217.73	263.45	259.98	250.64	248.93	248.47	248.28	243.8	243.8	207.5	197.9	197.9	204.9	202.2	212.8	210.8	213.4	213.4	213.4	213.4	213.4	213.4	213.4	213.4	213.4	213.4	213.4	213.4	213.4	213.4
Gasifier Prod Gas	113.15	139.74	141.11	130.21	127.94	133.29	137.81	139.0	121.6	119.7	100.15	103.3	177.4	177.4	180.0	180.0	180.0	180.0	180.0	180.0	180.0	180.0	180.0	180.0	180.0	180.0	180.0	180.0	180.0	180.0
Water	87.16	88.18	81.18	84.58	83.60	77.56	74.94	74.2	68.6	68.6	68.6	68.6	68.6	68.6	68.6	68.6	68.6	68.6	68.6	68.6	68.6	68.6	68.6	68.6	68.6	68.6	68.6	68.6	68.6	68.6
Unretained Char	6.46	6.10	3.10	4.07	3.94	4.30	8.89	9.9	6.14	4.22	3.04	3.4	4.7	6.0	10.33	9.0	9.0	9.0	9.0	9.0	9.0	9.0	9.0	9.0	9.0	9.0	9.0	9.0	9.0	9.0
Char U/O	13.78	31.34	33.81	31.79	33.54	18.23	22.56	23.9	23.8	14.99	19.89	23.1	16.2	21.1	21.9	19.8	19.8	19.8	19.8	19.8	19.8	19.8	19.8	19.8	19.8	19.8	19.8	19.8	19.8	19.8
Sour Gas	-	-	-	-	-	-	-	-	-	-	-	-	-	-	-	-	-	-	-	-	-	-	-	-	-	-	-	-	-	-
MEA Purge	-	-	-	-	-	-	-	-	-	-	-	-	-	-	-	-	-	-	-	-	-	-	-	-	-	-	-	-	-	-
EM Purge	-	-	-	-	-	-	-	-	-	-	-	-	-	-	-	-	-	-	-	-	-	-	-	-	-	-	-	-	-	-
Gasifier Acc.	-0.67	1.53	0.24	-1.27	-0.78	3.54	-0.31	-0.4	0.23	0.77	-0.23	1.5	0.3	0.0	1.23	1.24	-2.73	-3.13	4.95	-2.12	-0.10	-0.10	4.19	1.3	-	-	-	-	-	
NO Cleavage (B)	100	100	100	100	100	100	100	100	100	100	100	100	100	100	100	100	100	100	100	100	100	100	100	100	100	100	100	100	100	100
Syn Gas in Gasifier (ccm)	2637	3274	3141	3184	3097	3393	3116	3164	3013	3109	3355	3183	3543	3393	3793	3690	3654	3625	3625	3625	3625	3625	3625	3625	3625	3625	3625	3625	3625	
H ₂ /CO Ratio	4.77	3.49	3.34	3.41	3.48	3.44	3.60	3.58	3.40	4.28	5.08	4.0	5.04	4.9	5.0	5.04	5.0	5.0	5.0	5.0	5.0	5.0	5.0	5.0	5.0	5.0	5.0	5.0	5.0	5.0
H ₂ /CO in Prod. Gas	8153	2924	2928	2716	2558	3037	2493	2414	2337	2337	2183	2028	2323	2174	2323	2323	2323	2323	2323	2323	2323	2323	2323	2323	2323	2323	2323	2323	2323	2323
Syn Gas (B)	81.8	77.7	86.8	81.2	81.6	81.0	80.1	78.9	84.6	85.9	73.1	89.0	69.2	64.2	64.2	64.2	64.2	64.2	64.2	64.2	64.2	64.2	64.2	64.2	64.2	64.2	64.2	64.2	64.2	64.2
Syn Gas (C)	84.3	84.2	82.9	82.0	81.0	81.0	81.0	81.0	81.0	81.0	81.0	81.0	81.0	81.0	81.0	81.0	81.0	81.0	81.0	81.0	81.0	81.0	81.0	81.0	81.0	81.0	81.0	81.0	81.0	81.0
Syn Gas (D)	60.00	54.9	65.3	58.7	58.7	70.2	56.7	53.9	59.0	62.3	44.6	78.9	44.6	44.6	44.6	44.6	44.6	44.6	44.6	44.6	44.6	44.6	44.6	44.6	44.6	44.6	44.6	44.6	44.6	44.6
Conversion (B)	24.6	21.8	22.4	23.3	24.8	24.8	24.6	24.6	24.6	24.6	24.6	24.6	24.6	24.6	24.6	24.6	24.6	24.6	24.6	24.6	24.6	24.6	24.6	24.6	24.6	24.6	24.6	24.6	24.6	24.6
Steam Conv. (B ₂ O)	73.8	54.0	59.7	57.7	54.9	78.6	68.8	69.5	72.7	78.5	48.6	31.0	64.4	64.4	64.4	64.4	64.4	64.4	64.4	64.4	64.4	64.4	64.4	64.4	64.4	64.4	64.4	64.4	64.4	64.4
Carbon Conv.	197.3	161.0	183.6	169.3	169.0	181.0	210.9	184.0	177.6	111.4	211.2	233.0	413.0	652.0	611.0	342.0	327.0	410.0	483.0	520.0	381.6	347.4	348.0	347	347	347	347	347	347	
Ave.	8.0	8.5	8.7	8.2	8.0	8.5	8.8	8.1	8.1	9.1	10.3	9.3	16.9	19.8	22.9	14.4	12.4	15.6	17.3	22.0	14.4	27.8	31.9	14.5	14.5	14.5	14.5	14.5	14.5	
B-C	9.7	7.8	8.7	8.6	8.6	7.8	9.8	10.3	9.6	9.5	10.6	12.4	12.3	12.3	12.3	12.3	12.3	12.3	12.3	12.3	12.3	12.3	12.3	12.3	12.3	12.3	12.3	12.3	12.3	12.3
C-E	9.0	6.7	6.9	6.2	6.2	7.0	9.5	9.1	8.6	8.6	10.4	10.3	10.3	10.3	10.3	10.3	10.3	10.3	10.3	10.3	10.3	10.3	10.3	10.3	10.3	10.3	10.3	10.3	10.3	10.3
K-F	4.2	4.9	5.3	5.7	5.7	5.2	5.3	5.0	4.6	4.3	4.9	4.2	4.4	4.4	4.4	4.4	4.4	4.4	4.4	4.4	4.4	4.4	4.4	4.4	4.4	4.4	4.4	4.4	4.4	4.4
Bed Height (ft)	54.3	49.7	53.5	55.0	55.0	56.0	50.9	47.4	52.3	48.9	49.3	50.3	47.7	53.4	47.4	43.3	47.1	43.4	43.7	48.7	50.3	51.0	52.0	43.4	43.4	43.4	43.4	43.4	43.4	
Specific Resistance	0.33	0.34	0.38	0.33	0.34	0.28	0.41	0.43	-	0.42	0.39	-	0.34	0.33	0.44	0.49	0.46	0.47	0.47	0.47	0.47	0.47	0.47	0.47	0.47	0.47	0.47	0.47	0.47	
C Gasifier/Steam (mol/mol)	0.89	1.27	1.40	1.87	1.72	0.63	1.48	1.19	-	1.24	1.76	-	1.7	2.3	3.7	2.7	0.72	1.4	1.45	1.63	1.83	1.83	1.83	1.83	1.83	1.83	1.83	1.83	1.83	
C in Bed/Steam (mol/mol)	39.4	28.6	27.2	29.7	29.8	45.3	2.7	21.3	-	32.5	23.6	-	31.1	21.3	17.2	41.0	47.8	32.3	34.7	40.6	40.6	40.6	40.6	40.6	40.6	40.6	40.6	40.6	40.6	
Gasification Rate (B/hr)	16.24	13.62	12.31	12.64	12.66	14.39	15.20	15.8	15.8	15.8	17.16	18.87	13.8	18.3	18.9	20.3	19.0	17.3	19.3	19.3	19.3	19.3	19.3	19.3	19.3	19.3	19.3	19.3	19.3	
SCP Chg/lb C Prod	21.6	18.5	15.3	14.1	13.5	14.2	17.3	18.8	19.8	19.8	19.7	21.7	14.2	18.1	19.3	23.0	23.0	23.0	23.0	23.0	23.0	23.0	23.0	23.0	23.0	23.0	23.0	23.0	23.0	
Sup. Vol. (ft ³ /sec)	0.486	0.378	0.330	0.326	0.326	0.371	0.319	0.32	0.30	0.48	0.46	0.42	0.33	0.33	0.33	0.33	0.33	0.33	0.33	0.33	0.33	0.33	0.33	0.33	0.33	0.33	0.33	0.33	0.33	0.33
Solid Residence Time (hrs)	9.0	4.5	4.7	4.8	4.2	7.3	7.1	5.8	4.9	10.3	5.8	4.9	10.3	10.3	10.3	10.3	10.3	10.3	10.3	10.3	10.3	10.3	10.3	10.3	10.3	10.3	10.3	10.3	10.3	10.3
Approach to Equilibrium %	73	77	100	103	84	112	112	112	112	112	112	112	112	1																

TABLE 3.2-1 (cont inved)

POU MATERIAL BALANCE SUMMARY (RECONCILED)

Material Balance No.	50	51	52	53	54	55	56	57	58	59	60	61	62	63	64	65	66	67
Date	2-18	3-11	3-12	3-15	3-25	3-26	3-27	3-28	3-30	4-1	4-2	4-4	4-5	4-6	4-8	4-10	4-11	4-14
Row No Closure, X	109	102	97	84	94	102	101	102	96	93	100	94	91	93	91	86	87	90
<u>Operating Conditions</u>																		
Avg. Bed Temp., °F	1292	1299	1279	1272	1274	1281	1272	1285	1283	1281	1283	1279	1285	1283	1276	1271	1269	1267
Pressure, psia	505	512	512	513	504	505	506	504	502	500	500	500	500	501	500	500	499	501
Steam/Row Coal Ratio	1.4	1.5	1.5	1.5	2.0	2.0	1.9	1.7	1.7	1.6	1.9	1.8	1.8	2.0	1.9	2.0	2.7	1.8
<u>Feed Coal Properties</u>																		
Top Size, mesh	16	16	16	16	16	16	16	16	16	16	16	16	16	16	16	16	16	16
Avg. Part. Diam., X	-	210	220	230	210	130	130	150	140	160	130	170	200	150	130	170	150	150
X w k ² (A.S.)	6.9	6.2	6.8	6.4	6.4	7.0	7.8	7.3	7.2	7.2	6.5	6.6	6.9	6.9	6.2	6.6	6.4	7.2
<u>Inputs lbs/h</u>																		
Coal & Catalyst	349	363	349	338	369	385	371	399	409	409	402	391	397	388	409	382	353	386
Steam	124	124	119	124	114	122	119	130	130	132	121	120	122	114	127	119	91	122
Syn Gas	153	161	158	168	201	210	199	192	193	199	194	195	198	207	196	193	193	194
	72	78	72	47	53	54	53	77	87	87	82	76	60	77	75	72	78	70
<u>Outputs lbs/h</u>																		
Product Gas	344	363	349	340	435	500	551	496	461	441	400	392	397	389	413	383	352	384
Condensed Water	192	211	200	190	192	207	201	235	251	247	237	232	236	227	243	223	192	225
Intrinsed Char	111	116	113	113	144	140	133	124	124	119	129	121	121	126	126	121	136	122
Char Withdrawn	25	30	27	18	26	24	24	25	23	23	25	25	28	21	23	25	16	21
Accumulation	16	6	8	18	8	11	12	14	11	16	9	14	12	14	21	14	9	17
	5	0	0	-1	0	3	1	2	1	4	2	-1	0	0	-4	-1	1	2
<u>Performance Parameters</u>																		
Steam Conv., %	28	28	28	33	29	33	33	36	36	37	35	38	38	36	39	38	30	38
Carbon Conv., %	77	82	84	86	82	85	86	85	90	83	85	83	85	85	84	80	81	82
Gasification Rate, %/hr	41	52	44	44	30	43	53	50	62	54	58	68	66	79	61	49	50	49
SCF CH ₄ /lb C fed	19	20	20	18	16	16	16	18	20	17	18	16	16	16	15	14	16	16
CH ₄ in Dry, N ₂ Free PG, %	26	29	27	26	20	20	18	23	25	22	21	20	20	19	19	18	15	21
Approach to CH ₄ Equil., °F	84	46	57	42	88	67	111	74	64	90	85	81	96	97	107	116	128	89
Syn Gas Balance, %	64	58	62	74	83	88	91	77	71	77	79	85	83	84	90	92	88	86
<u>Bed Properties</u>																		
Avg. Bed Density, lbs/ft ³	15	14	13	12	16	19	21	17	18	16	16	13	13	12	13	10	9	12
Bed Height, ft	46	63	64	64	51	49	49	55	60	53	57	58	57	67	58	55	49	58
Bed Weight, lbs	371	384	443	443	435	500	551	496	461	441	498	414	412	375	406	295	234	375
Nominal Solids Residence Time, h	9	10	12	11	11	14	17	14	13	12	17	12	11	13	10	8	10	10
Top Sup. Vel., ft/s	0.4	0.4	0.4	0.4	0.5	0.5	0.5	0.5	0.5	0.5	0.5	0.5	0.5	0.5	0.5	0.5	0.4	0.5
<u>GMC Properties</u>																		
Bulk Density, lbs/ft ³	-	-	-	28	30	34	42	34	32	31	38	30	27	30	28	28	33	32
N/C Atom Ratio	0.12	0.17	0.17	0.20	0.12	0.21	0.34	0.24	0.30	0.22	0.29	0.21	0.22	0.32	0.22	0.12	0.15	0.19
Avg. Particle Diam., μ	-	220	190	160	150	280	130	110	112	90	100	90	90	210	120	140	100	90

The preoxidizer was generally operated at 350°F, 132 lbs feed per hour, 7200 SCFH of a 10 1/2% O₂ in N₂ mixture and four to six hour residence time. Due to intermittent operation of the preoxidizer and to mixing of the coal, it is difficult to associate a specific set of preoxidizer conditions with a given material balance period.

Material Balance Periods 1-5 and 10-12 were at 500 psia, but bed density and steam and carbon conversions were unacceptably low. For these reasons a lower pressure regime was investigated (MB 6-8 and 13-37). Although bed density and conversions generally remained relatively low during this period, operability of the pilot plant was demonstrated; a continuous run of thirty-three days was achieved in May and June 1980. During this period, bed densities as high as 17 lbs/ft³ were achieved and steam and carbon conversions of near 35% and 90% respectively were achieved (MB-20).

Beginning in August 1980, gasifier pressure was raised to 500 psia which led to numerous operating difficulties. In January 1981, a continuous run of nine days was carried out (MB 45-48). This period was characterized by a dramatically increasing bed density, from 14 to over 30 lbs/ft³, and high carbon conversion, over 95% at the end of the run.

During March and April 1981 a continuous demonstration run of twenty-three days was carried out under base case conditions.

3.3 Cold Model Studies

A cold model of the PDU was constructed to assist in troubleshooting solids flow problems as they arise in PDU operations. Throughout the startup and initial operation of the PDU, the transparent cold model proved valuable in providing visual understanding of many of the solids flow problem areas. A diagram of the cold model is shown in Figure 3.3-1. The unit consists of a fluidized bed reactor, a cyclone, an entrained char return system, and solids feeding equipment.

Most dimensions of the cold model are the same as the PDU except that the model gasifier is 14 feet in height versus the 83 feet of the PDU. This height difference should not affect the solids transfer studies. The inside diameter of the model reactor is 9-1/2 inches compared to 9-7/8 inches for the unit reactor. The inside diameter of the model dipleg is 2-5/8 inches which is identical to that of the PDU.

Polypropylene powder is the particulate solid used in the model. The particle density of the polypropylene is 44 lb/ft³ (0.70 g/cc) and the surface volume mean particle diameter is about 230 microns. These properties, as well as the shape factor for polypropylene, are similar to those of the gasified char produced in the small fluid bed gasifier (FBG). In addition, the negligible attrition of the polypropylene makes it a particularly good solid substitute for char for use over a period of time.

The areas requiring detailed experimentation were identified during preliminary operations. These included:

- Performane evaluation of solids feeding system
- Entrained char return system studies

Solids Feeding System Studies

In the PDU, coal is fed to the reactor in a cyclic manner from a lockpot with a volume of 0.1 ft³. First the lockpot is filled from above. The contents of the lockpot then flow through a vertical line into a 45° feed line and finally into the reactor. The coal feed rate is controlled by the frequency of the feed cycle. Figure 3.3-2 is a diagram of the feed system of the cold model. Dimensions of the model feed system are similar to those of the PDU except that the length of the 3/4 inch feed line is much longer in the PDU.

Successful solids feeding depends on proper valve sequencing, gas surge rate to the system, and purge location. Performance of the equipment was evaluated with respect to these operating variables and to reactor conditions including bed height and superficial gas velocity.

FIGURE 3.3-1

COLD MODEL OF GASIFICATION REACTOR SECTION OF PDU

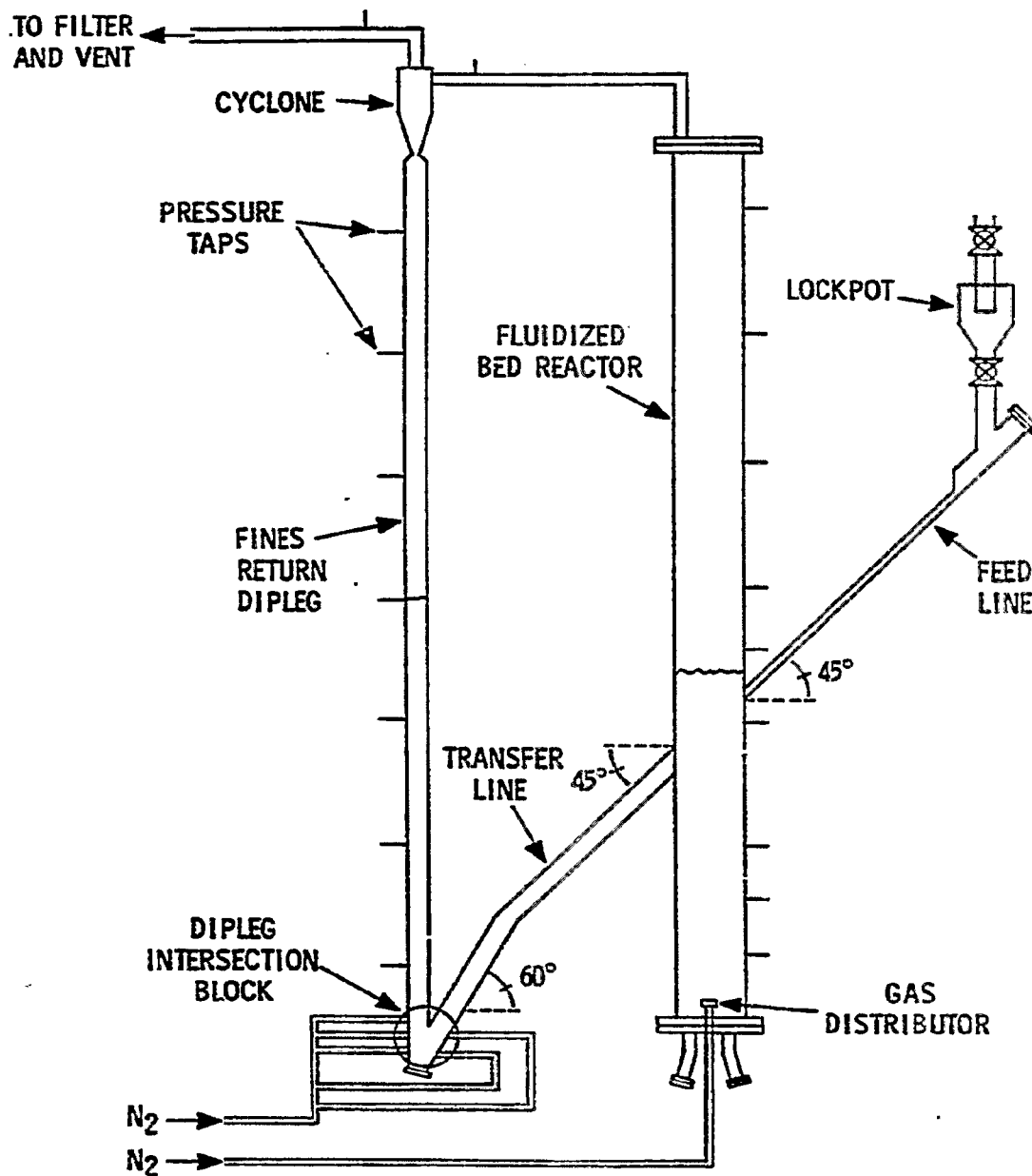
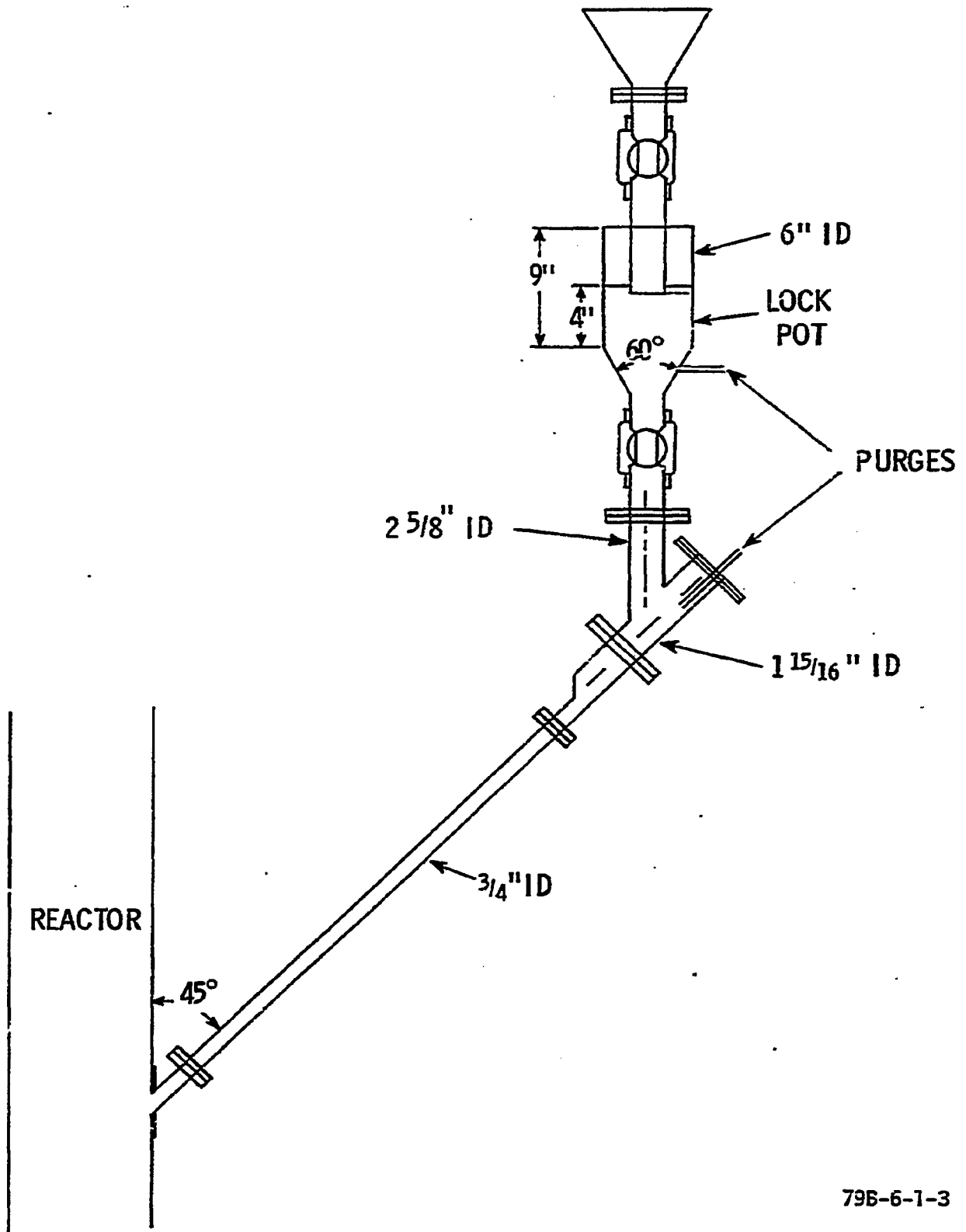


FIGURE 3.3-2
SOLIDS FEED SYSTEM FOR COLD MODEL



795-6-1-3

Feed Line Operation

The first experiments conducted were to determine whether solids from the reactor could be kept from backing up into the feed line. The effects of bed height above the feed point, superficial gas velocity in the reactor and gas purge rate to the feed line were examined.

The distance that the solids backed up from the reactor into the feed line was measured for reactor bed heights of 2, 3-1/2, 5, 6-1/2, and 8 feet above the feed point. The superficial gas velocity in the reactor was 0.45 ft/sec for each case. Higher bed heights forced solids farther up the feed line when there was no gas purge; however, a low flow of gas purged to the feed line from a tap located at the upper end of the 45° section of the line effectively eliminated the problem for all the bed height studies. Figure 3.3-3 shows the distance the solids backed up from the reactor as a function of bed height above the feed point and purge rate to the feed line.

A second set of experiments was carried out with a decrease in the reactor superficial velocity from 0.45 ft/sec to 0.11 ft/sec. The decreased superficial velocity reduced the solids backup in the feed line. The problem could be controlled in these cases by maintaining a low gas purge rate to the feed line as before. Figure 3.3-4 shows the results of experiments for two reactor superficial gas velocities with a bed height above the feed point of 8 feet.

The results of these experiments indicate that the problem of solids moving from the reactor into the feed line can be controlled by maintaining a gas purge so that the superficial gas velocity through the 3/4 inch line is at least 0.2-0.3 ft/sec.

Lockpot Operation

As mentioned earlier, solids feed rate is controlled by the frequency of the feed cycle. A catalyzed coal feed rate of 115 lbs/hr (the PDU design basis) would require one complete feed cycle every 140 seconds if the lockpot filled and emptied completely during the cycle. Experiments were carried out to determine how to operate the feed system in order to achieve the necessary cycle time. Initial experiments were designed to determine the length of time to empty the lockpot under different operating conditions.

The lockpot would not empty when the bottom valve was opened unless there was a gas purge directly to the lockpot of about 8 ACFH. At this low purge rate the lockpot drained erratically and occasionally would not empty completely. When the purge rate to the lockpot was increased above 8 ACFH, not only did the time required to empty the lockpot decrease but also the reproducibility of duplicate runs improved because the lockpot drained more smoothly. Purge location was very important in these experiments. A gas purge to the feed line below the lockpot was not as effective as a direct purge to the lockpot. Figure 3.3-5 shows how an increase in gas purge results in a decrease in the time required to empty the lockpot.

FIGURE 3.3-3

PURGE GAS REQUIREMENTS TO PREVENT SOLIDS FROM
BACKING UP INTO FEED LINE

EFFECT OF BED HEIGHT

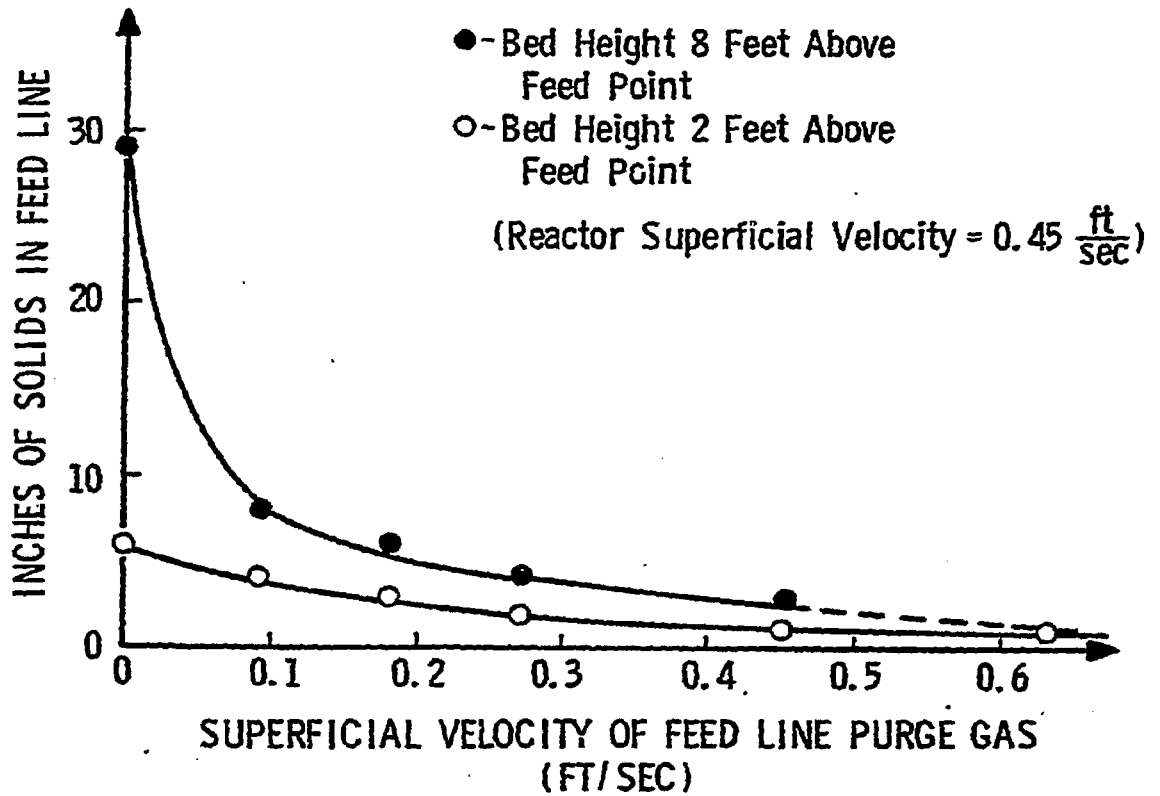


FIGURE 3.3-4

PURGE GAS REQUIREMENTS TO PREVENT SOLIDS FROM
BACKING UP INTO FEED LINE

EFFECT OF SUPERFICIAL VELOCITY IN THE REACTOR

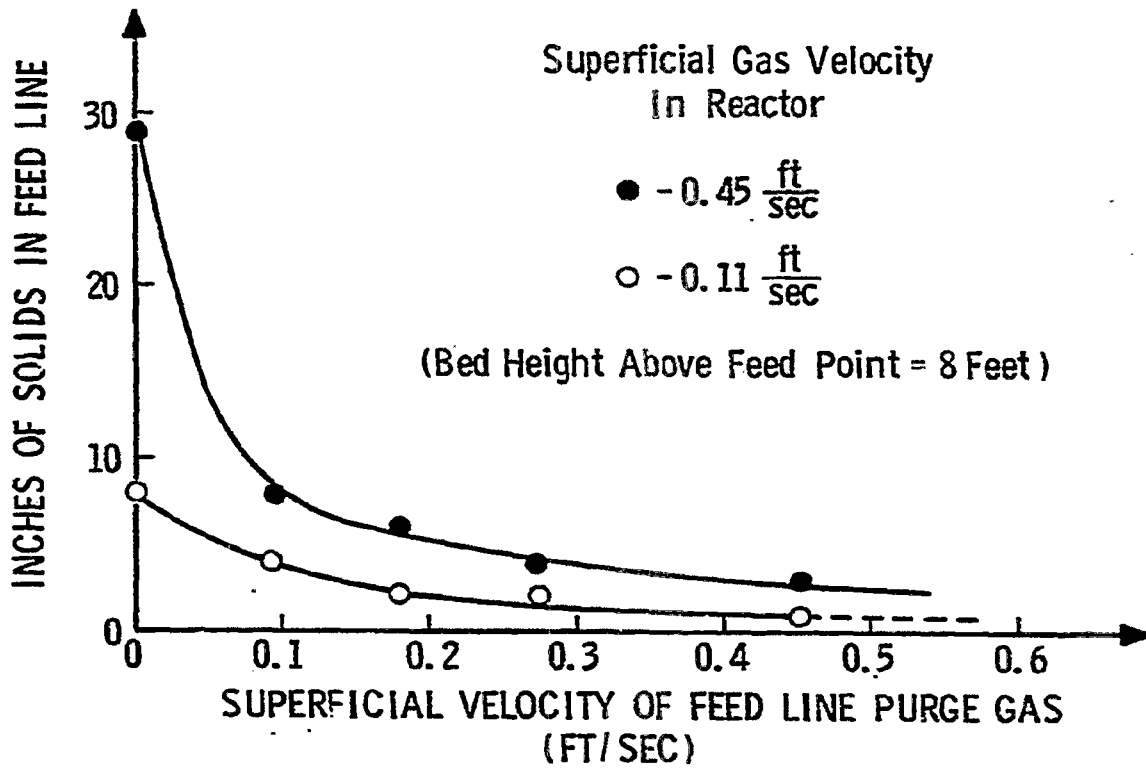
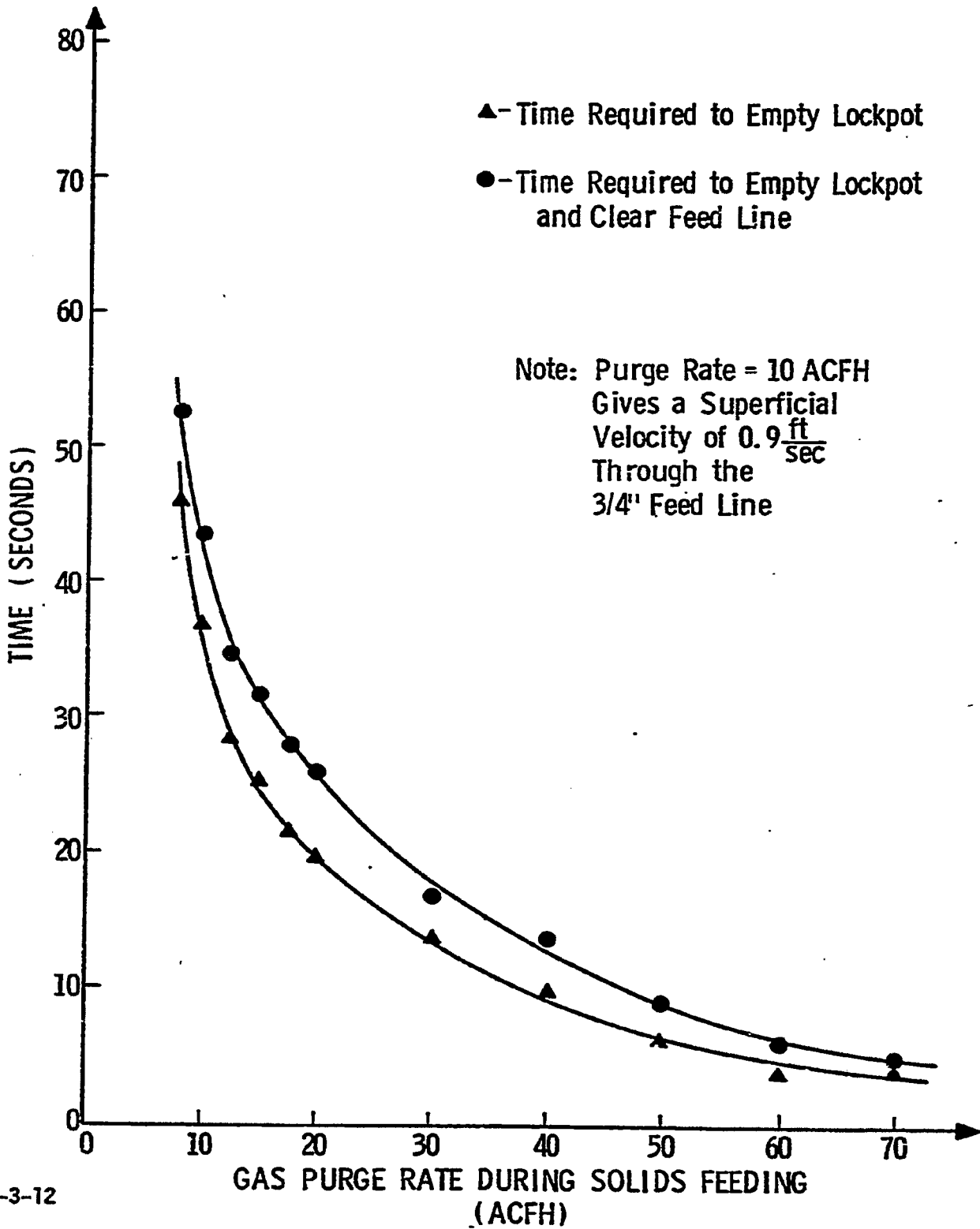


FIGURE 3.3-5

PURGE GAS REQUIREMENTS FOR FEEDING SOLIDS INTO THE
COLD MODEL



As shown in Figure 3.3-2, after the solids leave the lockpot, they travel through the feed line and into the reactor. The first part of the line is vertical with an inside diameter of 2-5/8 inches. It then goes through a 45° bend and into an eccentric reducer where the line is reduced to 3/4 inches inside diameter.

Experiments were conducted in the cold model to determine how fast the solids would move through the feed line and into an actively fluidized bed. The feed line on the cold model is six feet long, which is considerably shorter than that of the PDU. The longer feed line in the PDU should not have a significantly higher resistance to solids flow than the feed line in the model because most of the resistance to solids flow results from bends and constrictions in the line and the resistance of solids flow into the fluidized bed. These effects are present in both the cold model and the PDU.

It has already been shown that solids will back up from the fluidized bed into the feed line unless a small gas purge is maintained. When feeding solids into the reactor, a higher purge rate of at least 12 ACFH was needed. This is more than the minimum purge required to empty the lockpot. If the purge rate was below 12 ACFH, the solids did not move into the reactor from the 3/4 inch section of the feed line as fast as they drained from the lockpot and so the level of solids in the feed line rose. Frequently this resulted in compacting and bridging of solids which caused the feed line to plug.

At purge rates in the range of 12 to 18 ACFH, the solids moved through the feed line and into the reactor in spurts. Above 18 ACFH there was enough gas moving with the solids to keep the material from compacting and maintain smooth solids flow. Figure 3.3-5 shows the time required to empty the lockpot and to clear the feed line for a range of gas purge rates from 10 to 70 ACFH. Higher purge rates gave greater solids mass flow rates into the reactor.

Recommendations for PDU Operation

The results from the cold model indicated that it is possible to achieve smooth operations and the required coal feed rates to the PDU by supplying gas purges to the feed system. When the lockpot is being filled or the bottom lockpot valve is closed, purge gas must enter directly into the feed line below the lockpot at a rate of at least 2.5 ACFH (0.25 ft/sec) to keep solids from moving from the reactor up into the feed line. When the bottom lockpot valve is opened to feed solids, a gas purge directly into the lockpot in the range of 20-60 ACFH is needed to drain solids from the pot. Once the solids are out of the lockpot, a gas purge is required to feed the solids into the fluidized bed. This gas can be supplied through the lockpot purge if the bottom lockpot valve remains open.

Entrained Char Return System Studies

As demonstrated by past operations of fluid bed catalytic coal gasification pilot plants, solid particles are entrained in the gas stream leaving the reactor. Some of these particles are less than 50 microns in diameter and have a higher carbon content than char in the fluidized bed. The difference in the carbon content of the two types of char can be attributed to relatively low residence times for the smaller particles which leave the reactor more quickly than larger particles. The fine char carried overhead in the gas stream comes from two sources. Part of it is char from fine feed coal particles, while the rest is the product of attrition of larger particles in the fluidized bed. This fine, high carbon char should be returned to the reactor for further gasification in order to achieve a higher overall carbon conversion and higher process efficiency.

On the PDU, the system to return the entrained char to the reactor consists of a cyclone, dipleg, intersection block and a transfer line as shown in Figure 3.3-1. The cyclone and dipleg are not inside the reactor due to its relatively small diameter. The fact that the cyclone and dipleg are external to the reactor results in a special design for the dipleg return which is characteristic of smaller fluidized bed units. At the bottom of the dipleg is an intersection block from which a transfer line leads back to the reactor. The transfer line begins at an angle 60° from the horizontal, goes through a 15° bend and enters the reactor at 45° from the horizontal.

The design of the solids return system is such that the rate of char return to the bed should be controlled by pressure balance. If the solids in the dipleg, intersection block, transfer line, and reactor are properly fluidized, the system should behave like a manometer. As char falls into the dipleg from the cyclone, the level of solids rises in the dipleg, causing an increase in static pressure at the bottom of the dipleg. If this pressure is greater than that at the point at which the transfer line enters the reactor, then the solids should move from the dipleg into the reactor.

The cold model is equipped with a return system like the one previously described. Internal dimensions of the model are nearly identical to those of the PDU except that the length of the dipleg is approximately 14 feet compared to the 70 foot dipleg on the PDU. Initial experiments on the model were designed to investigate solids flow behavior in the dipleg and transfer line.

Dipleg Operation

The char in the dipleg should be fluidized slightly above minimum fluidization if they are to flow smoothly through the intersection block and into the transfer line. Too little purge gas in the cold model resulted in solids slumping, compacting, and bridging in the dipleg, causing solids flow to stop. Once this occurred, it was difficult to reestablish a fluidized state in the dipleg. Sudden increases in gas flow caused plugs of solids to move up the dipleg like a piston. This behavior was accompanied by an increase

in pressure drop which was characteristic of flow through a packed bed. The most successful procedure for refluidizing compacted solids was to slowly increase and decrease the gas flow to the dipleg. This resulted in a smooth transition from a packed to a fluidized bed. Excess gas flowing up the dipleg led to slugging in the bed of dipleg.

The gas flowing through the dipleg must pass through the base of the cyclone and out the top with the gas from the reactor. The original cyclone design called for a throat diameter of 13/16 inch, as shown in Figure 3.3-6. This would mean that the superficial gas velocity of the dipleg purge gas would be ten times greater through the cyclone throat than through the 2-5/8 inch ID dipleg. Experiments were carried out to determine whether cyclone performance was affected by the dipleg purge gas passing through the cyclone.

Dipleg purge rates above 3 ACFH resulted in cyclone plugging. Beginning at the throat of the cyclone, the polypropylene powder clung to the walls of the cyclone cone and accumulated there until it plugged completely. The cyclone did not plug when the dipleg purge rate was below about 3 ACFH. These results indicate that gas flowing up through the cyclone does affect cyclone performance. The total purge gas rate to the dipleg should be kept to a minimum during operation of the PDU to avoid high superficial gas velocities at the cyclone throat which would interfere with cyclone performance.

A change was made in the cyclone design for the PDU based on these experiments. The throat diameter was increased from 13/16 inches to 1-1/8 inches, reducing the gas superficial velocity by nearly one-half in the throat of the cyclone. This should reduce the frequency of cyclone plugging.

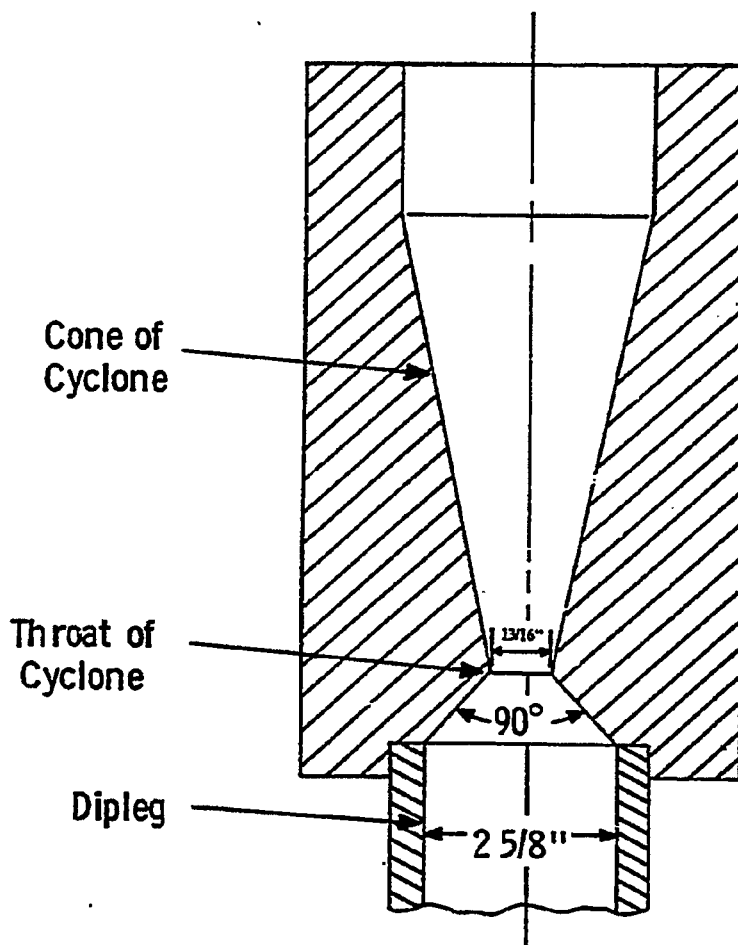
Transfer Line Operation

Solids must travel up the inclined transfer line to return to the reactor from the dipleg. Gas must be fed into the transfer line to keep the particles moving in order that they will flow back into the reactor. Gas was supplied to the transfer line at various rates and the behavior of the solids in the inclined tube was observed.

Gas superficial velocities below about 0.20 ft/sec in the transfer line resulted in stagnant solids along the entire length of the line. As the superficial gas velocity was increased, solids activity increased along the top of the transfer line while solids in the bottom of the line remained stationary. Solids in the top half of the 60° section of the line began to slug at a superficial gas velocity of about 0.3 ft/sec. Slugs broke up at the angle between the 60° and 45° sections and solids in the 45° section were motionless. Gas velocities of about 1-2 ft/sec. were required to eliminate zones of stagnant solids along the bottom of the transfer line. At these gas velocities, the solids slugged up the line and then flowed back down the bottom of the line. Generally, the solids activity in the 60° part of the transfer line was greater than that in the 45° part of the line.

FIGURE 3.3-6

ORIGINAL CYCLONE DESIGN - BOTTOM OF CYCLONE



Intersection Block Studies

Subsequent experiments on the cold model were designed to determine how to control dipleg and transfer line fluidization simultaneously by varying purge gas rates and locations. The purge gas can enter the system at any of five locations in the intersection block. A diagram of the intersection block with the purge locations numbered 1 through 5 is shown in Figure 3.3-7. Based on the experiments described above, most of the gas entering the fines return system at the intersection block should travel up the transfer line. High gas flow rates are required in the sloping line to eliminate zones of stagnant solids. Purge gas flow traveling up the vertical dipleg should be kept to a low value to avoid interference with cyclone performance but should be enough to keep the solids in the dipleg fluidized.

Each of the intersection block purges is equipped with a sliding tube that can be moved into the intersection block as indicated in Figure 3.3-7. Sliding the tube into the intersection block to different positions results in different gas flow patterns.

Purge location #3 gave the best control of flow up either the dipleg or the transfer line but not to both simultaneously. When the tube was extended beyond the entrance to the dipleg, most of the gas went into the transfer line and there was little solids motion in the dipleg. When the tube was retracted to the wall (as shown in Figure 3.3-7), most of the purge gas flowed up the dipleg. Purge location #2 produced gas flow patterns similar to location #3 but control was not as good. Most of the purge gas flowed up the transfer line in the most extended tube position, but there was intermittent slugging in the dipleg which did not occur when purge location #3 was used. Purges #1 and #4 supplied purge gas only to the vertical dipleg at all tube extensions. Purge #5 gave little control of flow up the transfer line. Most of the purge gas flowed up the dipleg when the tube was extended to greater than 1/3 of the maximum extension into the intersection block.

These results indicate that purge location is important in controlling fluidization of the fines return system. A purge directly into the base of the transfer line is required to supply high gas flow rates to the transfer line while allowing negligible amounts of gas into the dipleg. Required flow to the dipleg can be supplied from other purge locations in the intersection block.

FIGURE 3.3-7
DIPLEG INTERSECTION BLOCK
COLD MODEL VERSION

